Impact Sensors for Use with Electronic Fuzes

December 1975

TR-1728—Impact Sensors for Use with Electronic Fuzes—by Harry J. Davis

U.S. Army Materiel Command
HARRY DIAMOND LABORATORIES
Adelphi, Maryland 20783

The findings in this report are not to be construed as an official Department of the Army position unless so designated by other authorized documents.

Citation of manufacturers' or trade names does not constitute an official indorsement or approval of the use thereof.

Destroy this report when it is no longer needed. Do not return it to the originator.

UNCLASSIFIED

SECURITY CLASSIFICATION OF THIS PAGE *(When Data Entered)*

REPORT DOCUMENTATION PAGE		READ INSTRUCTIONS BEFORE COMPLETING FORM
1. REPORT NUMBER HDL-TR-1728	2. GOVT ACCESSION NO.	3. RECIPIENT'S CATALOG NUMBER
4. TITLE *(and Subtitle)* Impact Sensors for Use with Electronic Fuzes		5. TYPE OF REPORT & PERIOD COVERED Technical Report 6. PERFORMING ORG. REPORT NUMBER
7. AUTHOR(s) Harry J. Davis		8. CONTRACT OR GRANT NUMBER(s) DA: 1W662616AH77
9. PERFORMING ORGANIZATION NAME AND ADDRESS Harry Diamond Laboratories 2800 Powder Mill Road Adelphi, MD 20783		10. PROGRAM ELEMENT, PROJECT, TASK AREA & WORK UNIT NUMBERS Program: 6.26.16.A
11. CONTROLLING OFFICE NAME AND ADDRESS Commander US Armaments Command Rock Island, IL 61201		12. REPORT DATE December 1975 13. NUMBER OF PAGES 55
14. MONITORING AGENCY NAME & ADDRESS(*if different from Controlling Office*)		15. SECURITY CLASS. *(of this report)* Unclassified 15a. DECLASSIFICATION/DOWNGRADING SCHEDULE

16. DISTRIBUTION STATEMENT *(of this Report)*

Approved for public release; distribution unlimited.

17. DISTRIBUTION STATEMENT *(of the abstract entered in Block 20, if different from Report)*

18. SUPPLEMENTARY NOTES

HDL Project No. A77542
AMCMS Code: 662616.11.EH700

19. KEY WORDS *(Continue on reverse side if necessary and identify by block number)*

Fuzes
Impact sensors
Artillery shells

20. ABSTRACT *(Continue on reverse side if necessary and identify by block number)*

The factors affecting the design of mechanical impact elements were surveyed. Forces encountered during impact with raindrops and with various target materials, particularly water, are discussed. Trends in the design of the element itself are presented.

DD FORM 1 JAN 73 1473 EDITION OF 1 NOV 65 IS OBSOLETE

UNCLASSIFIED

SECURITY CLASSIFICATION OF THIS PAGE *(When Data Entered)*

CONTENTS

APPENDICES

FIGURES

FIGURES (CONT'D)

TABLES

1. INTRODUCTION

Mechanical impact elements are used in electronic time and proximity fuzes as a selectable option or as a backup, should the electronic fuze fail. These elements must meet various requirements, some of which apply to all mechanical impact devices, and some of which apply only to those used in electronic fuzes. This report discusses various aspects of impact sensor design during electronic fuze projects of interest to the US Army. It supplements data on impact fuzes contained in existing reports.[1] Since completely electronic target surface sensors are discussed elsewhere, they are not treated here.[2]

2. DESIGN CONSIDERATIONS

A major factor in the design of impact sensors is the specification of those target characteristics that determine the forces acting on the sensor. Targets of interest to the Army include hard ones such as metal, rock, concrete, and macadam; and relatively soft ones such as soil, sand, and water. Of primary interest to this study are the characteristics of soft targets, since these set the sensitivity requirements for the impact sensors. Forces generated when a projectile impacts earth are difficult to define, since they depend on soil characteristics such as composition, compaction, water content, and temperature. These parameters can vary across the surface of the impact area, with the depth of penetration and with time.

Appendix A summarizes selected information on the forces generated during soil penetration. Appendix B summarizes information recently developed on water penetration.

The range of impact velocities and angles of interest to this study is defined in figure 1; data are shown for a variety of rounds used by the Army. The data are taken from appropriate firing tables. The impact angle is measured from the horizontal, and it is assumed that the target is horizontal. The impact velocity may vary for a given impact angle (data are shown as a shaded area), since both muzzle velocity and quadrant elevation can be variables in a firing. The highest velocity (fig. 1) is 3000 ft/s, and the lower limit is approximately 200 ft/s. Gun-projectile combinations are capable of velocities outside this regime, but the data presented are considered typical of fuzed projectiles. The impact angles vary from grazing to 90 deg. Mortar shells have impact velocities with an upper limit of about 700 ft/s and a lower limit of about 200 ft/s. Their impact angles, under the assumptions specified, are greater than 40 deg. The 20-mm projectile and the 40-mm grenade have low-impact velocities and angles.

---

[1] *Proceedings of the Fuze/Munitions Environment Characterization Symposium (U), Vol. I, II, US Army Munitions Command, Picatinny Arsenal (1972). (CONFIDENTIAL)*

[2] *Fuzes, Electrical, Proximity, Electrical, Part One (U), Army Materiel Command Pamphlet 706-211 (1963). (CONFIDENTIAL)*

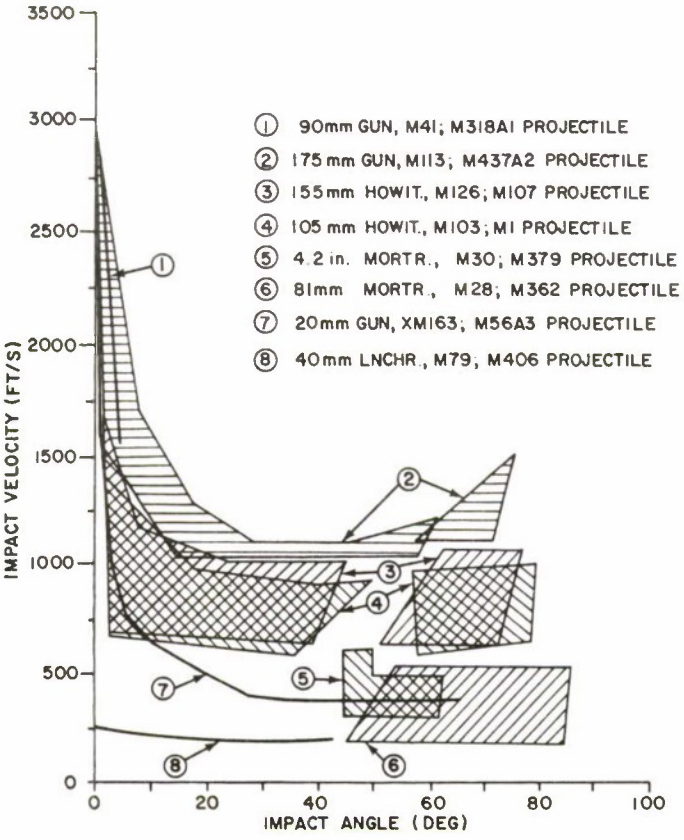

Figure 1. Impact velocity and angle characteristics of some US Army Ordnance projectiles.

In addition to these factors, other ballistic conditions must be considered in impact element design. These include the setback forces that occur during firing, forces generated by spin, and any in-flight perturbations after arming due to air resistance, flight instabilities, and impacts with rain, jungle canopy, and foliage. The fuze should not function due to these perturbations, and special mechanisms have been designed to insure their not functioning on, for example, raindrops.[3] The technique most commonly used is to decrease the sensitivity of the sensor. Doing so, however, reduces the probability of functioning at low impact velocities, at low impact angles, or on soft targets.

Data on impacts with trees or tall grass are being gathered,[1] and study of this information should lead to more accurate estimates of the forces generated and to means of dealing with them.

---

[1] *Proceedings of the Fuze/Munitions Environment Characterization Symposium (U), Vol. I, II, US Army Munitions Command, Picatinny Arsenal (1972). (CONFIDENTIAL)*

[3] *W. J. Lohninger, Concepts and Basic Principles of the Selective Sensitivity or Density Integrating Fuze Head, Picatinny Arsenal TR-4125 (1970).*

A mathematical model of projectile flight through a rainstorm has been developed.[4] This model uses empirical data defining the size distribution of raindrops in various types of rainstorms.[5] It can be assumed that the probability of hitting a raindrop in a specific interval of time is the same as in any preceding or succeeding interval of equal length. Poisson distribution is obtained by use of this distribution. The size of the impacting raindrop is chosen randomly.

A computer program of the model takes into account the effects of stagnation pressures generated during a projectile flight. Design characteristics of the impact element (such as size, bias, spring constant, and critical displacement for functioning) are inputs to the problem. The form of the data output can be selected as element displacement as a function of time: the number of fuze functions for a specified number of runs or the maximum displacement experienced by the element in each of its runs. The program has been used in the design of an impact switch and is available from the author for future applications.

3. MECHANISM RESPONSE

The force applied to the impacting projectile is not necessarily the force applied to the impact sensor, since the dynamic response of the projectile influences the behavior of its components. Some insight into this can be gained by the study of the response of the accelerometers used in the experimental impact tests (app A).

The impact sensors for ordnance applications most widely accepted use the energy generated during an impact to actuate a mechanical element that is part of the mechanical initiator or electrical switch that fires a detonator. The energy driving the mechanical element must act against various elastically and plastically deforming devices, such as springs or collars, that serve to bias the element against spurious inputs, e.g., shell vibrations and raindrop impacts. The energy driving the element against stab detonators must be large enough to work against the biasing element and close the gap and also accelerate the element to the critical velocity necessary to reliably initiate the detonator. Data deal with the optimized design of initiators for stab detonators taking critical velocity into account.[6] Data indicate also a critical velocity in the functioning of percussion detonators.[7] A switch contact connected directly to an electric detonator in a circuit must remain closed until enough current flows through the detonator for initiation.

---

[4] *A. Hausner and R. Kushlis, Monte-Carlo Simulation of PD Fuze Function during a Rainstorm, Harry Diamond Laboratories TR-1643 (October 1973).*

[5] *E. A. Mueller and A. L. Sims, Calibration and Comparison of Simulated Rainfields with Natural Rains, Illinois State Water Survey Report R1993 (1971).*

[6] *G. Lowen, Spring-Driven Primer Striker Study, City College [New York] Research Foundation Final Report, Contract DAAG-39-68-C-0026 (1970).*

[7] *S. Zarra, Investigation of Sensitivity Level of Primer Percussion M61, Picatinny Arsenal TR-1-60 (1960).*

A study of existing designs (app C) indicates that impact elements can be categorized as follows:

(a) Inertially driven elements that depend on the linear or angular deceleration of the round, with resulting relative motion between the impact switch elements.

(b) Pressure-driven elements that depend on the impact force acting directly on one element to either plastically or elastically deform the biasing element.

(c) Stress-wave driven elements that depend on the shock waves generated in the fuze material during the impact.

Although all three effects may act in varying degrees in any one design in a given application, engineers usually design with only one of these concepts in mind.

3.1 Inertially Driven Elements

Inertial elements are relatively small and operate in any location inside the fuze. They function reliably over a wide variety of projectile impact and target conditions. Unfortunately, an inertial element does not function as rapidly as a pressure-actuated element under low-velocity, soft-target impacts, expecially when the inertial element is biased to withstand in-flight vibrations and rain. Inertial switches are usually chosen for fuze applications on the basis that they are tested designs that have been used in previous fuzes. New impact element designs require extensive field testing, since there are only general rules to assist in their design. A means of defining target sensitivity requirements, as well as appropriate biasing levels, would therefore help in the design of impact fuzes.

Kornhauser has proposed one means of defining the sensitivity of inertial elements,[8] and this concept has been analyzed.[1] He suggested that the velocity of an inertial switch element on functioning be plotted against the peak applied acceleration. Figure 2 shows the results of an analysis on a switch similar to those described by Thiebeau and Lucey.[9] The velocity of the moving member on functioning is plotted against the peak acceleration of the applied pulse. The asymptotic approach to the velocity axis can be expected, since a minimum impulse imparts just enough momentum to the moving member to move it to its functioned condition. The minimum velocity is that associated with this momentum. The acceleration asymptote represents the bias applied to the moving member. Figure 2 shows two curves for different forcing functions, one for a rectangular pulse and the other for a half-cycle sine driving the element. Both curves approach the same asymptotes; the difference between the two curves is small elsewhere. The functioning of the switch described here is governed

---

[1] *Proceedings of the Fuze/Munitions Environment Characterization Symposium (U), Vol. I, II, US Army Munitions Command, Picatinny Arsenal (1972). (CONFIDENTIAL)*

[8] *M. Kornhauser, Prediction of Firing Depths of Impact Fuzes, Degradation Effects Program, Aberdeen Proving Ground, Methodology and Evaluation Working Group Report 4 (1969).*

[9] *R. Thiebeau and G. Lucey, Jr., Inertial Impact Switches for Artillery Fuzes, Part I: Development, Harry Diamond Laboratories TM-72-18 (July 1972).*

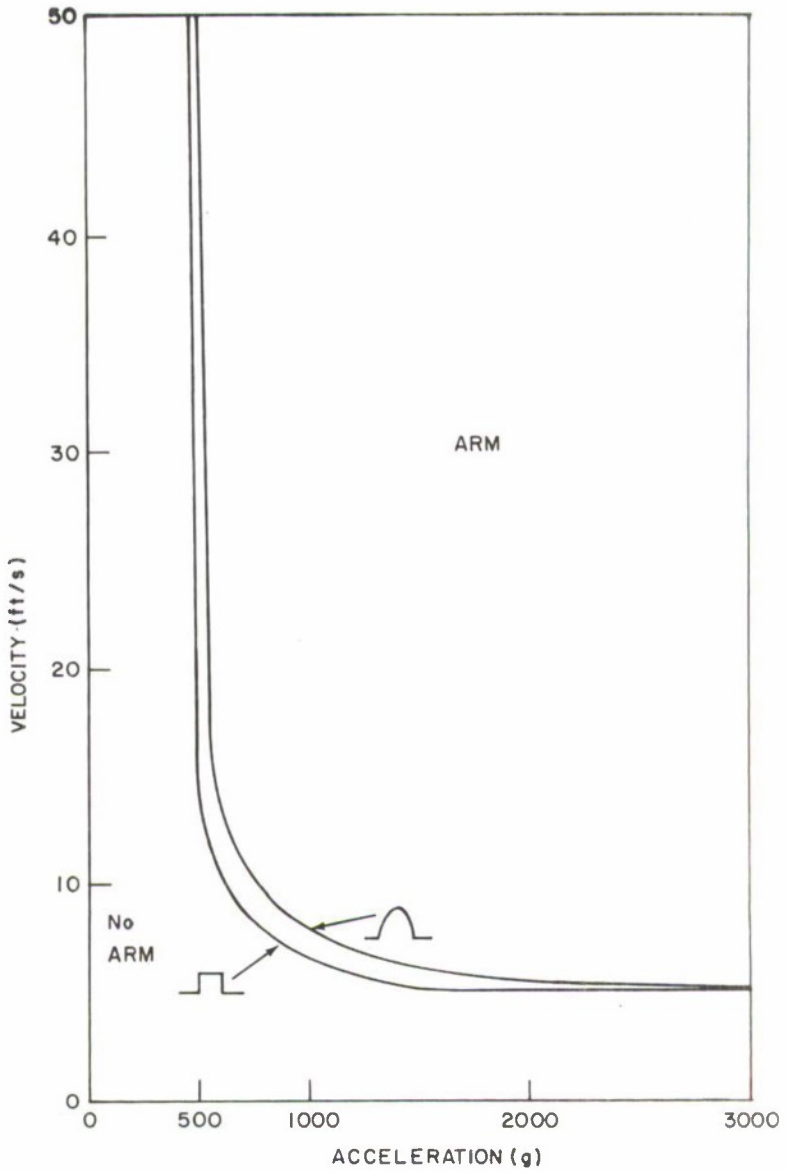

Figure 2. Sensitivity diagram for impact switch.

by the distance that the moving element must travel. A sensitivity curve for an element that must have a critical velocity in order to function has different characteristics, depending on the shape of the driving pulse.[1]

[1]*Proceedings of the Fuze/Munitions Environment Characterization Symposium (U), Vol. I, II, US Army Munitions Command, Picatinny Arsenal (1972). (CONFIDENTIAL)*

3.2 Pressure-Driven Switches

Pressure-driven switches are relatively inexpensive, are small, and function rapidly when force is exerted upon them. They must be located so that the impacting surface makes contact with a part of the switch. The response of a pressure-activated switch member was recently investigated.[10] In this work, flat plates mounted on the front of projectiles were fired into water. The time between water impact and switch closure was recorded by means of a trailing wire. The switch closure time lasted tens of microseconds.

3.3 Stress-Wave Actuated Switches

Switches activated by the stress waves generated during an impact can potentially act quickly at low velocities on soft targets and be small. One of the major deficiencies in the design of such a switch is the small amount of experience with it.

The general principles underlying a one-dimensional analysis of the waves generated during a projectile-target interaction are given in appendix D. That analysis shows (fig. D-1) the pressures that would be developed behind shock waves in different projectile materials (phenolic, aluminum, and iron) when they impacted perpendicularly to different target materials (sand, ice, water, snow) at a velocity of 200 ft/s. During impacts at different velocities, pressure can be generated by shifting the origin of the projectile material curves to the appropriate value. However, the curves are relatively linear in the regime shown, but their nonlinearity becomes more significant at higher values.

Since figure D-1 is based on unevaluated information, it is difficult to determine if the pressures shown for the two types of dry sand truly differ. The data for wet and dry sand come from the same source,[11] however, so it is reasonable to assume that wetting sand greatly increases the pressure beyond that which can be expected from impact on dry sand. The relatively low pressure that can be expected from an impact on snow is apparent from the figure. The state of this snow (density, state of compaction, etc.) is not specified.[11]

The pressures shown for a water impact occur whether the target is a raindrop or the ocean. The amplitude of the pressures generated during a raindrop impact, however, soon drops because of tensile waves generated at the impact surface. This limitation to the total energy imparted to a body during an impact suggests a means of discriminating between raindrop and water target impacts.

An all-mechanical stress-wave actuated switch has been studied.[12] In this work, experimental data obtained while different target materials were fired onto switches of various designs corroborated the major features of a theoretical analysis. More work is needed to

---

[10] *R. Wasser, Impact Switch Tests, US Naval Ordnance Laboratory TR-71-225 (1971).*

[11] *J. S. Rinehart, Compilation of Dynamic Equation of State Data for Solids and Liquids, U. S. Naval Ordnance Test Station TP 3798 (1965).*

[12] *D. Neily, Investigation of Stress-Wave Impact Switches for Electronic Fuzing, Harry Diamond Laboratories TM-73-8 (July 1973).*

define the effect of many types of target and project materials, switch location in the fuze, and the effect of impact angle between projectile and target. Available information indicates that the designs tested perform satisfactorily during medium-velocity, normal impacts on hard targets, but perform marginally at low-velocity, oblique impacts on soft targets. For this reason, a switch that uses low-energy stress waves to initiate switching action was designed (app E). In the fuze circuit in which this switch is used, the detonator is initiated from stored electrical energy, and raindrop impacts, etc., are discriminated against by electronic logic.

4. SUMMARY AND CONCLUSIONS

Some factors affecting the design of impact switches used in electronic proximity fuzes were studied.

4.1 Forcing Functions

A major hindrance in designing a sensitive impact element is in-flight collisions of the fuze with raindrops. A mathematical model of fuze performance in a rainstorm has been described. This model offers promise not only as a design tool, but also as a means of determining the statistical performance of a new design. Raindrop impacts initiate shock waves in the projectile. An impact switch that operates solely on the amplitude of the forcing function, such as a simple piezoelectric crystal, and that actuates the fuze on a low-velocity impact with water is therefore likely to function on a high-velocity impact with a raindrop.

The state of the art in analyses of earth impacts has been outlined. Recent investigations show promise in accurately describing the projectile's trajectory in relatively soft targets, but have limited use in describing forces acting on the projectile at the target's surface. In addition, the model has unknown usefulness on shells, angles, shapes, and target materials that differ from those used in obtaining the basic data. Scaling studies may overcome these limitations.

Investigations into simple equations of motion, such as represented by the Poncelet equation, have yielded results that express the relative sensitivity of various switch designs. This sensitivity appears to be due not only to the multidimensional nature of impact, but also to the effects during cratering, travel through the target near the earth's surface, and the like. However, the use of a simple equation of motion with a drag coefficient and a velocity squared dependence has yielded results usable for engineering design.

Phenomena occurring as a projectile impacts a solid surface are still a matter of investigation, particularly for oblique impacts. The experimental data presented here indicate that the forcing function may be a spike pulse of high amplitude and short duration (thousands of gravities, a few microseconds), a spikelike pulse of

lower amplitude and longer duration (tens of microseconds), or a function that increases over a period of milliseconds to an amplitude of hundreds of gravities. The type of pulse and its amplitudes and time durations depend on the nose shape, projectile characteristics, target material, impact angle, and projectile velocity. A semiquantitative understanding of the interrelation of these parameters would provide fuze designers with a powerful tool. The use of a drag coefficient to study the effect of the above parameters would be a logical start.

Well-defined drag coefficients applicable to water impacts have been presented. These permit the modeling of impact element behavior with some degree of confidence. This modeling is convenient, since water is not only common as a target, but also quite uniform over the surface of the earth. It can be used as a standard target so that the results of different calculations and the measured performance of switches of different design can be compared. Such a procedure would be particularly powerful if combined with sensitivity curves, i.e., experimental functioning rates being shown superimposed on analytically determined peak acceleration-velocity change curves.

4.2 Element Design

(a) Pressure-actuated switches appear to be the most widely used means of initiating a function in impact fuzes. They can be made to be quite sensitive and quick acting. The impact element must be placed at or near the front of the fuze and can be subject to cumulative deformation. Experimental work has been outlined[10] on the time-dependent deformation of flat plates used as switch elements.

(b) Inertially actuated switches are used as backup elements in many fuzes. They can be made to function independently of impact angle and may be placed anywhere in a fuze structure. As a class, inertially actuated switches do not appear to be as sensitive or as quick acting as pressure-actuated switches. The presentation of experimental field test results on sensitivity curves would simplify the comparison of various inertial impact-switch designs.

(c) Few, if any, impact switches have been successfully designed to function on stress waves. Work on the design of a mechanical stress wave switch has been outlined.[12]

(d) Various switches have been built that generate electrical energy. This energy has been used both as power for the detonator and as an information signal to open an electronic gate.

(e) The large effort in designing mechanical impact elements suggests that further efforts will produce very small improvements. Attempts to improve the performance of general-purpose impact switches might be more fruitful if more effort were expended on electro-mechanical systems. One principle that could be applied to such a

---

[10] *R. Wasser, Impact Switch Tests, US Naval Ordnance Laboratory TR-71-225 (1971).*

[12] *D. Neily, Investigation of Stress-Wave Impact Switches for Electronic Fuzing, Harry Diamond Laboratories TM-73-8 (July 1973).*

system is to use a very sensitive detector that goes off on soft targets at low velocities and that uses both duration and amplitude to discriminate between raindrops and legitimate water targets. A design using this principle is presented in appendix E.

ACKNOWLEDGEMENTS

I gratefully acknowledge discussion with Harry Diamond Laboratories staff members David Overman, Louis Richmond, John Scales and Naval Surface Weapons Center staff member Jack Goeller, the permission of Sandia Corporation, Texas A. & M. U., and the General Dynamics Corporation to reproduce the appropriate data given in the text. John L. Baldwin, NSWC, coauthored appendix B. Philip Ingersol, HDL, designed the circuit for the impact sensor described in appendix E.

LITERATURE CITED

(1) Proceedings of the Fuze/Munitions Environment Characterization Symposium (U), Vol. I, II, US Army Munitions Command, Picatinny Arsenal (1972). (CONFIDENTIAL)

(2) Fuzes, Electrical, Proximity, Electrical, Part One (U), Army Materiel Command Pamphlet 706-211 (1963). (CONFIDENTIAL)

(3) W. J. Lohninger, Concepts and Basic Principles of the Selective Sensitivity or Density Integrating Fuze Head, Picatinny Arsenal TR-4125 (1970).

(4) A. Hausner and R. Kushlis, Monte-Carlo Simulation of PD Fuze Function During a Rainstorm, Harry Diamond Laboratories TR-1643 (October 1973).

(5) E. A. Mueller and A. L. Sims, Calibration and Comparison of Simulated Rainfields with Natural Rains, Illinois State Water Survey Report R1993 (1971).

(6) G. Lowen, Spring-Driven Primer Striker Study, City College [New York] Research Foundation Final Report, Contract DAAG39-68-C-0026 (1970).

(7) S. Zarra, Investigation of Sensitivity Level of Primer Percussion M61, Picatinny Arsenal TR-1-60 (1960).

(8) M. Kornhauser, Prediction of Firing Depths of Impact Fuzes, Degradation Effects Program, Aberdeen Proving Ground Methodology and Evaluation Working Group Report 4 (1969).

(9) R. Thiebeau and G. Lucey, Jr., Inertial Impact Switches for Artillery Fuzes, Part I: Development, Harry Diamond Laboratories TM-72-18 (July 1972).

(10) R. Wasser, Impact Switch Tests, US Naval Ordnance Laboratories TR-71-225 (1971).

(11) J. S. Rinehart, Compilation of Dynamic Equation of State Data for Solids and Liquids, U. S. Naval Ordnance Test Station TP 3798 (1965).

(12) D. Neily, Investigation of Stress-Wave Impact Switches for Electronic Fuzing, Harry Diamond Laboratories TM-73-8 (July 1973).

APPENDIX A.--FORCES ACTING ON A PROJECTILE DURING SOIL IMPACT

Considerable work has been done to define what happens when a projectile hits a soil target. Unfortunately, most of the studies of a generalized nature have been in regimes of low-impact velocities (0 to 10 or 20 ft/s) or in the hypervelocity (multithousand feet per second) regimes. Past work in the velocity regime of significance to conventional artillery impacts (200 to 3000 ft/s) has been specialized studies for such purposes as estimating soil properties from penetration data[1]* or for defeating projectile penetration.[2] From studies such as these it is difficult to extract information on the impact forces acting on a shell. Information that is available is outlined here.

One of the most thorough experimental studies of projectile penetration was by Allen et al,[3] of the motion of a 50-caliber projectile through a box containing sand instrumented with a number of breakable wires. The nonreal nature of the prepared target was offset by the time-resolved nature of the data. One of the observations was that the projectile's trajectory can be unstable while the projectile is in the target. This was also observed in a study of the trajectory of small arms ammunition in water.[4]

The investigation by Allen et al,[3] indicated also that there were two regimes of significance in projectile penetration. The researchers identified the projectile velocity as the parameter defining these regimes and suggested that one penetration law governed when the projectile velocity was higher than the local sonic velocity in the target material, whereas another law held when the projectile velocity was less than the sonic velocity. A detailed study into penetration depths made by the Sandia Laboratories[5] also indicated two velocity regimes. Experimental penetration[6] indicated that particle penetration depth decreased with increasing impact velocity. No mechanisms to explain these phenomena were put forward.

A recent study into target trajectory phenomena involved the firing of 20- and 155-mm projectiles into sand and soil.[7] As with Allen's[3] work, breakable wires were used to determine the projectile's trajectory as a function of time. A mathematical model was developed. Portions of the projectile were not in contact with the target material during penetration, cratering affected initial impact, and surface effects lessened the retarding forces on the top of the projectile when it was close to the surface of the target. Such flow separation influenced the path of the projectile.

Recent experiments have gathered low velocity deceleration-time data.[1,8-10] Figures A-1 to A-5, tracings taken from these references, are meant to show general trends. Table A-I lists test conditions and target and projectile characteristics. All impacts were approximately normal to the ground, except for shots (d) and (e) of figure A-5, which specifically show a projectile approach angle (θ) and an angle of attack (α). Horizontal velocity information is given in some of

---

**See Literature Cited for all references in appendix A (p. 24).*

the figures to indicate small variations in the approach angle. The information given on instrumentation, mounting, and data processing is usually very sparse. This sparseness is unfortunate, since questions about frequency response and the number of degrees of freedom of the system underly data interpretation. The ratios of projectile length to diameter (L/D) shown should be viewed with the knowledge that many US Army gun and howitzer projectiles range from 4.4 to 4.9, whereas many mortars range from 5.5 to 7.7. The ratio of the weight of the projectile to its projected area (W/A) ranges from 1.7 to 4.7 lb/in.^{2} for many Army projectiles.

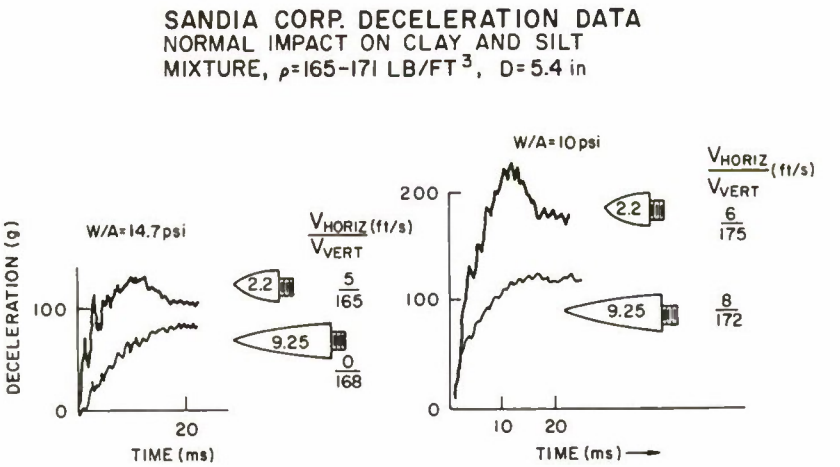

Figure A-1. Deceleration data, ogive impact on clay and silt.

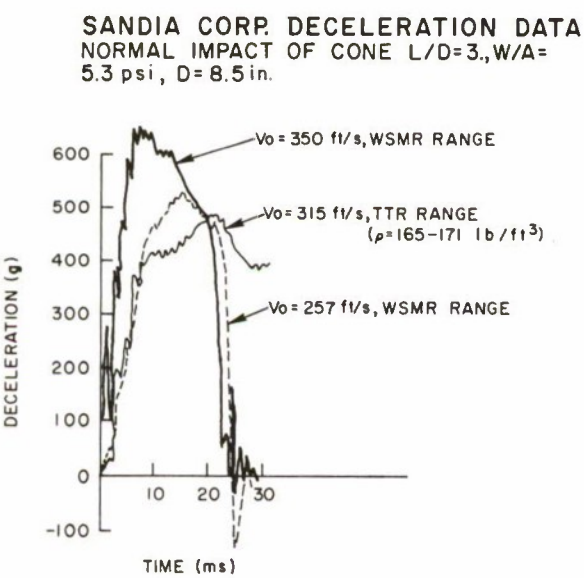

Figure A-2. Deceleration data, cone impact on test ranges.

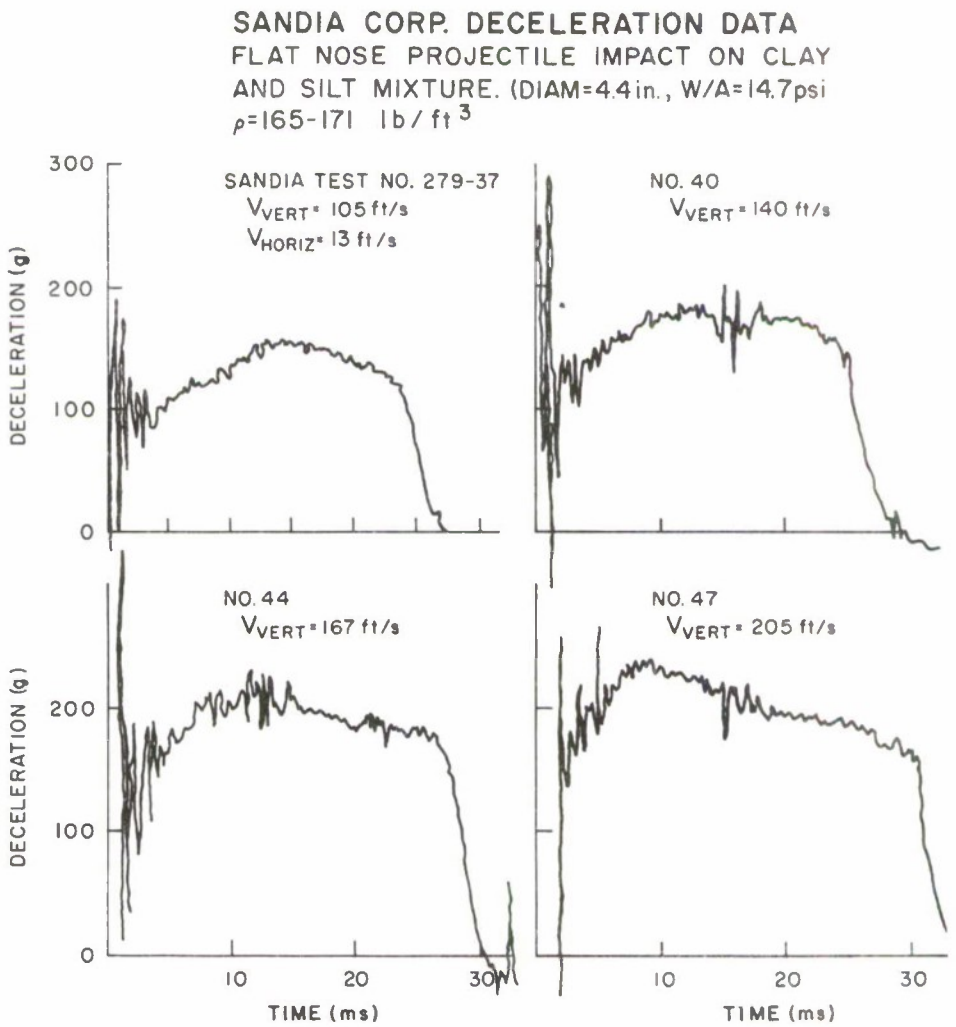

Figure A-3. Deceleration data, flat nose impact on clay and silt.

The characterization of the target material in table A-I is inexact. The place where the sample was taken, the density of the soil, and the number of blows needed to drive a standard stake 1 ft are given in the basic references but have limited applicability to solving dynamic penetration problems.

The data of figure A-5 need further explanation. The projectile used was equipped with terrabrakes. These are fins protruding at right angles to the body of the projectile that stop it after a specific penetration depth. The large downward-going peaks in figure A-5 are due to the impact of the terrabrakes. The angles in figure A-5 are the impact angle between the projectile's trajectory and the earth (θ) and the angle of the projectile's axis with its trajectory (α).

APPENDIX A

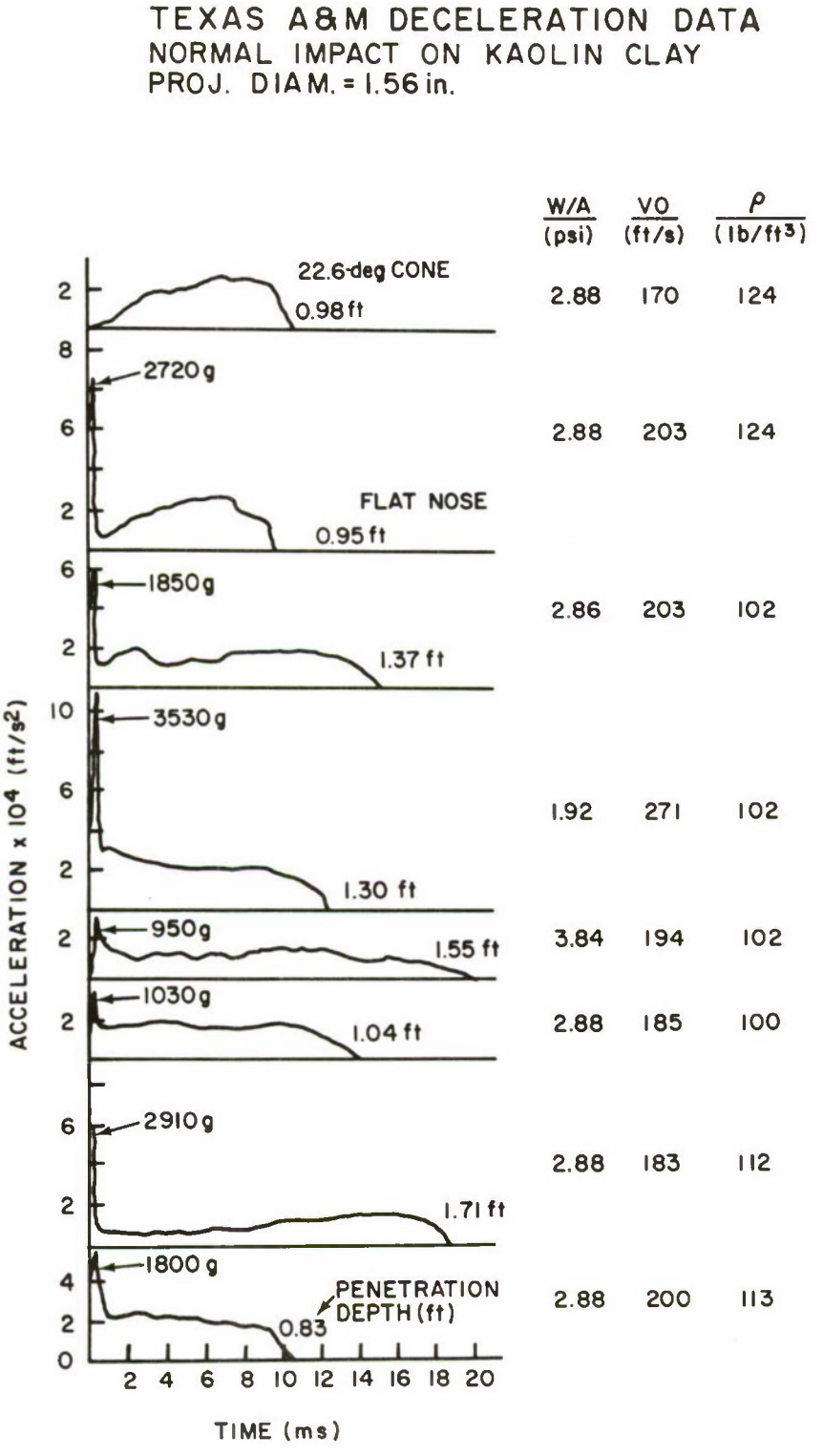

Figure A-4. Deceleration data, flat nose and cone impact on clay.

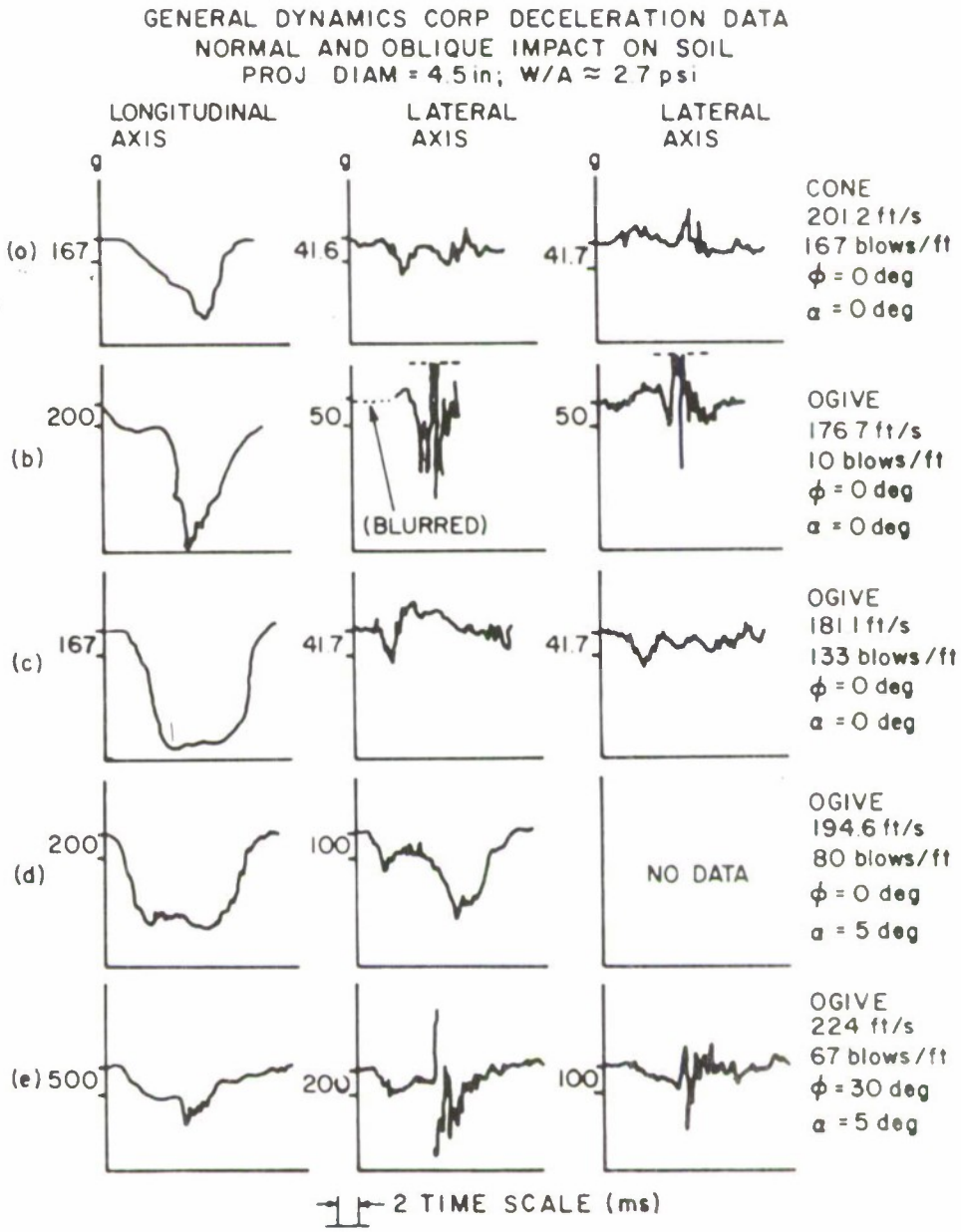

Figure A-5. Deceleration data, cone and ogive impact on soil.

TABLE A-I. CHARACTERISTICS OF IMPACT DATA, PROJECTILE, AND TARGET

Figure	Source	Impact data characteristics			Projectile characteristics			Target characteristics	
		Test technique	Accelerometer instrumentation	Impact velocity (ft/s)	Ratio of projectile length to diameter	Ratio of projectile weight to area (psi)	Nose shape	Type	Properties
A-1	Sandia Corp.[1]	Dropped from helicopter with parachute	6-kHz accel., mounting unknown, parachute pulls telemetry antenna; 1.05-kHz filter used	165 to 175	14.2, 14.7	10, 14.7	Ogive, 2.2 & 7.25 CRH, 5.4-in. base diam	Clay-silt mixture	Tonopah Test Range (TTR), soft soil
A-2	Sandia Corp.[2]	Same as A-1	Same as A-1	257, 315, 350	3	5.3	Cone, 25.5-in. long; 8.5-in. base diam	Same as A-1	White Sands Missile Range, hard soil; TTR, soft soil
A-3	Sandia Corp.[1]	Same as A-1	Same as A-1	105 to 205	9.68	4.4	Flat nose, 4.4-in. diam	Same as A-1	TTR, Soft soil
A-4	Texas A&M[3]	Gas-gun-shot projectile into specially prepared target	Accel. and mounting unknown, hardwire telemetry	170 to 203	12.05 to 13.90	1.92 to 2.88	Flat nose and 22.6-deg cone, 1.56-in. base diam	Kaolin clay	Density = 4 to 7 lb/ft^3
A-5	General Dynamics[4]	Gas-gun-shot projectile into earth, terra-brakes used	20-kHz accel., mounted on longitudinal plate, hardwire telemetry	177 to 224	Unknown	2.72	Ogive, 11.25-in. radius and cone, 6.75 in. long; 4.5-in.-diam	Unknown	Dynamic penetration test = 10 to 167 blows/ft

[1] *C. W. Young and G. Ozanne, Sandia Report SC-RR-66-306A (1966).*
[2] *C. W. Young, Sandia Report SC-DR-70-302 (1970).*
[3] *L. Thompson et al, Texas A&M Report on Contract 48-7432 (1969).*
[4] *C. Ingels and R. Sholtis, General Dynamics Report (1972).*

Consideration of the figures indicates the following:

(a) The higher the impact velocity, the higher the peak deceleration (fig. A-2).

(b) The harder the target material, the higher the peak deceleration (fig. A-4).

(c) The lower the W/A the higher the deceleration (fig. A-1).

(d) The blunter the nose, the higher the deceleration (fig. A-1).

(e) The blunter the nose, the faster the rise time of the deceleration pulse (fig. A-1, A-4); both cones and ogives produce curves that are relatively monotonic, but increasing bluntness and impact velocity tend to produce spikes and perturbations on the record.

(f) Flat noses induce sharp spikes in the deceleration record. Figure A-4 has no spike for the 22.6-deg cone impact, but there is a spike in the flat-nose data. Further, figure A-3 shows a number of spikes that correspond to "ringing," which becomes more pronounced with increasing impact velocity. The large initial spike could be caused by the acceleration of a relatively large amount of target material by the blunt nose of the projectile, by a relatively high-amplitude stress wave propagated through the projectile after impact, or by both. The ringing shown could be caused by the excitation of the projectile, of the measuring instruments, or of both.

(g) Oblique impacts amplify the lateral response of components mounted in the projectile (fig. A-5).

Many of these observations can be explained in terms of the drag equation (eq B-2):

$$M \frac{d^2x}{dt^2} = - \frac{1}{2} \rho C_D A V^2$$

or

$$\frac{d^2x}{dt^2} = - \frac{1}{2} \rho \frac{C_D g}{(W/A)} V^2 .$$

Acceleration depends directly on velocity and inversely on the W/A. Material properties, such as hardness, would affect the drag coefficient, C_D, as would projectile geometry such as the shape of the projectile's nose. In addition, a blunt-nosed projectile would generate a forcing function with a sharp rise time, which would excite the shell and its contents into vibration.

Theoretical investigations into shell impacts with earth-type targets are usually macroscopic penetration studies. The technique is to assume an equation of motion for the projectile. The constants in this equation are determined by integrating and maximizing the resulting distance equation to yield a penetration depth. Expressing

the penetration depth in terms of impact velocity yields an equation that can be fitted to experimentally gathered data. Robertson[2] compiles many of the equations of motion used in ordnance work. The equation that has received the most attention is the Poncelet equation, which was originally written as

$$MX = a + b\dot{X}^2$$

where

M is the projectile mass, X is the projectile displacement, and a and b are constants.

The constant term on the right side of the equation could be interpreted as dealing with the force needed to penetrate the target material's surface. The velocity-squared term is a conventional drag-coefficient dependency.

The constants a and b in the Poncelet equation are usually determined experimentally by the technique previously described. Robertson[2] lists "a" and "b" for various earth materials. The constants[11] for soft, medium, and hard earth are probably as good as any, since earth materials vary widely over the surface of the earth and with depth.

The Poncelet equation, as written above, predicts that the instantaneous force applied to the projectile on impact would be the maximum force applied to the system. The experimental data for cones and ogives do not support this picture. One way of overcoming this difficulty is to write the Poncelet equation as

$$M\ddot{X} = A(a' + b'\dot{X}^2)$$

where A is the area of the projectile exposed to the target material expressed as a function of penetration depth.

One investigation used this form of the equation, on the assumption that the projectile upon impact was effectively a flat plane of varying area.[12] The earth was assumed to be an incompressible fluid, permitting the use of classical drag coefficient theory. The mathematical model included the effects of lift and spin. A similar investigation used three coupled Poncelet equations with the varying projectile area to describe the projectile's motion in three dimensions. Empirically determined drag coefficients were used.[13]

Kornhauser[8] used a conventional drag equation, i.e., a Poncelet equation without the constant "a." He used drag coefficients that are a function of penetration depth. An analytic expression for spheres and empirical data for ogives, both bodies penetrating water, were used in the investigation. A ballistic density was introduced into the analysis to account for target materials other than water. This approach has been extensively used in impact switch function studies.[14]

An equation of recent attention is

$$M\ddot{X} = a_1 + a_2 X + a_3\ddot{X}.$$

Coefficients for low-velocity impacts (30 to 300 ft/s) into sand and clay for cone, ogive, and flat-nosed bodies have been gathered[6] for this equation.

The mathematical model developed with the 20-mm and 155-mm firings[7] uses drag coefficients to account for normal and tangential resistance pressures. The resulting force acting on the projectile varies with the area in contact with the target material. Analytic terms described the force needed to part the soil and sand target material and to account for target-projectile friction and flow separating effects. Cratering and surface effects are controlled by the two-dimensional computer program, which expresses the mathematical model. Preliminary work, including comparision of measured and calculated trajectories, was done on a three-dimensional model, which includes the effect of projectile spin.

APPENDIX A.--LITERATURE CITED

(1) C. W. Young and G. Ozanne, Compilation of Low Velocity Penetration Data, Sandia Laboratories Report SC-RR-66-306A (1966).

(2) H. Robertson, Terminal Ballistics, Report of the National Research Council, Committee for Passive Protection Against Bombing (1941).

(3) W. A. Allen et al, Dynamics of a Projectile Penetrating Sand, Parts I and II, J. Appl. Phys. 28 (1957), 370, 1331.

(4) H. Steves and B. Noonan, The Performance of Small Arms Ammunition when Fired into Water, US Naval Ordnance Laboratory TR-70-174 (1970).

(5) C. W. Young, Depth Penetration for Earth Penetrating Projectiles, Proceedings Journal Soil Mechanics and Foundation Division, ASCE 95, No. SM3, Proceedings Paper 6558 (May 1969), 803 (see Sandia Laboratory Report SC-DR-67-60).

(6) B. Rohani, Fragment and Projectile Penetration Resistance of Soils, Army Engineer Waterways Experiment Station Miscellaneous Paper S-61-12 (1973).

(7) F. Lascher et al, Projectile Impact and Penetration Forcing Functions—Engineering Study, AVCO Corporation Interim Final Report on Contract DAAA21-71-C-0517 (1972).

(8) L. Thompson et al, Effect of Soil Parameters on Earth Penetration of Projectiles, Texas A&M Research Foundation Technical Report to Sandia Laboratories on Contract 48-7432 (1969).

(9) C. Ingels and R. Sholtis, Grasshopper AVM Terradynamic Test Program Results, General Dynamics, Electrodynamic Division Report (1972).

(10) C. W. Young, Terradynamic Development of a Low Velocity Earth Penetrating Projectile, Sandia Laboratories Report SC-DR-70-302 (1970).

(11) M. P. King and R. D. Heidenreich, Penetration and Cratering Data for the MK81 Low Drag General Purpose Bomb (U), US Naval Ordnance Laboratory TR-70-184 (1970). (CONFIDENTIAL)

(12) S. H. Chu and F. K. Soechting, Dynamic Investigation of Grazing Shell, Picatinny Arsenal TM-1945 (1971).

(13) J. Kovacs and S. H. Chu, Forcing Functions for the High Performance Point Detonating Fuze Program, Picatinny Arsenal Information Report ESL-IR-483 (1970).

(14) J. Kovacs, Experimental and Predicted Firing Depths of Point Initiating into Snow, Mud, Water and Earth (U), Picatinny Arsenal TR-4095 (1971). (SECRET)

APPENDIX B.--FORCES ACTING ON A PROJECTILE DURING WATER IMPACT

by

J. L. Baldwin, US Naval Surface Weapons Center, White Oak, MD
and H. J. Davis, Harry Diamond Laboratories

B-1. INTRODUCTION

The forces acting on a projectile when it impacts a water target are described here. This information will enable an engineer to estimate the performence of fuze components used in such a projectile. The study was based on recent work by the US Navy.[1]

A projectile impacting water must accelerate the "added mass" of water in contact with the nose. This process is accompanied by compression and expansion waves of varying strengths that are propagated through the water. In the resulting flow pattern around the projectile, a cavity often forms about its nose; the size and duration of the cavity depend on the hydrodynamics of the problem. Other factors affecting the motion of a projectile within the target are the frictional forces generated as the projectile moves through the water and the natural buoyancy of the projectile. The degree to which the motion of the projectile is influenced by each factor is determined by the geometry of the projectile and by the initial condition of the problem. To treat every possible situation in detail is an intractable problem. The technique resorted to here is to use impact drag coefficients during the impact phase based on empirical data gathered under specified conditions. These coefficients may be used in generalized situations, provided their limitations are understood and are observed.

A projectile's stability affects it motion (not considered here). An ordnance projectile is designed to traverse the air in a specified manner; spin is often used to maintain its stability. The drastic change when the projectile enters the thousand-times-more-dense water causes the projectile to become inherently unstable. In addition, a motion, or "whip," about the projectile's lateral axis frequently results when it enters water. This whip phenomenon[2,3] is under study.

B-2. MOTION IN WATER

The one-dimensional motion of a projectile in water can be described by considering an inertially fixed control volume. The basic equation may be written as[4]

---

[1] *V. Dawson and A. Seigel, The State-of-the-Art of Water Entry Technology (U), US Naval Ordnance Laboratory TR-70-209 (1970). (CONFIDENTIAL)*

[2] *B. L. Noonan and H. K. Steves, The Performance of Small Arms Ammunition when Fired into Water, US Naval Ordnance Laboratory TR-70-174 (1970).*

[3] *J. O. Gurney, A Preliminary Study of the Mechanism of Water Entry Whip of 20° Cone Nosed Models, US Naval Ordnance Laboratory TR-66-148 (1966).*

[4] *J. L. Baldwin, An Experimental Investigation of Water Entry, Ph.D Thesis, University of Maryland, College Park, MD (1971).*

APPENDIX B

$$-\frac{d(M+m)u}{dt} + (Mg-B)\sin\theta = \frac{1}{2}\rho C_D A u^2 . \qquad \text{(B-1)}$$

The meanings of the symbols are listed at the end of this appendix.

Equation (B-1) involves masses and constants that are independent of entry velocity. In actuality, the values of the various terms depend on this parameter. A basic problem is, therefore, to estimate their functional dependence. The problem can be simplified considerably by noting that artillery and mortar shells and small rockets normally do not displace much water upon impact. Thus, the m term in equation (B-1) may be dropped. In addition, the projectiles are subjected to forces that are large with respect to the forces caused by their weight and volume. Thus, the second term on the left side of equation (B-1) is eliminated. With these approximations, equation (B-1) may be written

$$-M\frac{du}{dt} = \frac{1}{2}\rho C_D A u^2 \qquad \text{(B-2)}$$

and the problem now is evaluating the functional dependencies of the drag coefficient.

The velocity used in equation (B-2) is the instantaneous velocity of the projectile. When impact phenomena are considered, however, the impact velocity, u_0, can be used over an extended range, since shell velocity normally changes slowly in water. Estimates of the error involved in the use of a constant velocity can be obtained from equation (B-2) by changing variables from time to distance.

$$\frac{du}{dS} = \frac{1}{2}\frac{\rho}{M} C_D A u .$$

Integrating and rearranging yields

$$\frac{u}{u_0} = \exp\left[\left(-\frac{1}{2}\right)\left(\frac{\rho}{M}C_D A S\right)\right] . \qquad \text{(B-3)}$$

The actual velocity change experienced by the shell during its penetration can be calculated by equation (B-3).

Equation (B-3) can be arranged to yield

$$S = -\frac{2M}{\rho C_D A}\ln\left(\frac{u}{u_0}\right) . \qquad \text{(B-4)}$$

Equation (B-4) yields estimates of the penetration depths for various impact velocities.

The drag coefficients in this report are based on the area of the projectile's reference diameter. Thus, the drag force experienced by a 105-mm shell with an ogive nose is calculated by the appropriate drag coefficient for the ogive, and the area is calculated on the basis of a 105-mm diameter. If the drag force is due to a combination of factors, the area used is that appropriate to the geometry of each part. Thus, if the 105-mm ogive had a flat on its nose, the drag coefficient would be that appropriate to the flat, and the area would be based on the diameter of the flat. The total drag force would be the sum of the force due to the flat nose and the force due to the ogive.

B-3. DRAG COEFFICIENTS OF PROJECTILES IMPACTING WATER

B-3.1 Oblique Entry of Disk-Cylinder Projectiles

The total drag coefficient, C_D, is due to all the forces acting along the longitudinal axis of the projectile that oppose its forward motion. It is the sum of the transient (C_{DT}) and of the steady state (C_{DS}) drag coefficients.

The C_{DT} is proportional to the increase in added mass caused by the water surface. Its effect is maximum at the air-water interface and usually becomes negligible after a penetration of several body lengths. The C_{DS} is related to the rate that added mass is transferred from the body to its cavity or wake, the rate being governed by cavity formation factors, friction, etc. In any given instance, the C_{DS} varies from zero to its final value, this final value being the final value of the C_D. The C_{DS} is a variable, but it gets its name because its final value is steady or constant.

The final value of the C_{DS} is independent of entry angle for all shapes. The C_{DT} for disk-cylinders was found to be a single function multiplied by the tangent of the product of the projectile diameter and the cotangent of the entry angle.[4] Further, the distance penetrated is related to the product of the projectile diameter and the cotangent of the entry angle. These functional dependencies and some experimental data are shown in figure B-1. This method of characterizing disk-cylinders gives good agreement with experimental data from entry angles of 15 deg to nearly vertical entry. The cotangent dependence makes the drag coefficient extremely sensitive to angular variations near vertical impact.

Maximum quantities experienced under these conditions have been found[4] to be

$$C_{D'max} = 0.79 + 0.93 \tan \theta \qquad \text{(B-5)}$$

$$S\left(C_{D'max}\right) = 0.61 \ (D \cot \theta) \qquad \text{(B-6)}$$

---

[4] *J. L. Baldwin, An Experimental Investigation of Water Entry, Ph.D Thesis, University of Maryland, College Park, MD (1971).*

where $S(C_D, max)$ is the depth of penetration associated with C_D, max. Equation (B-5) is plotted in figure B-2. The first term of equation (B-5) is the C_{DT} for a disk-cylinder.

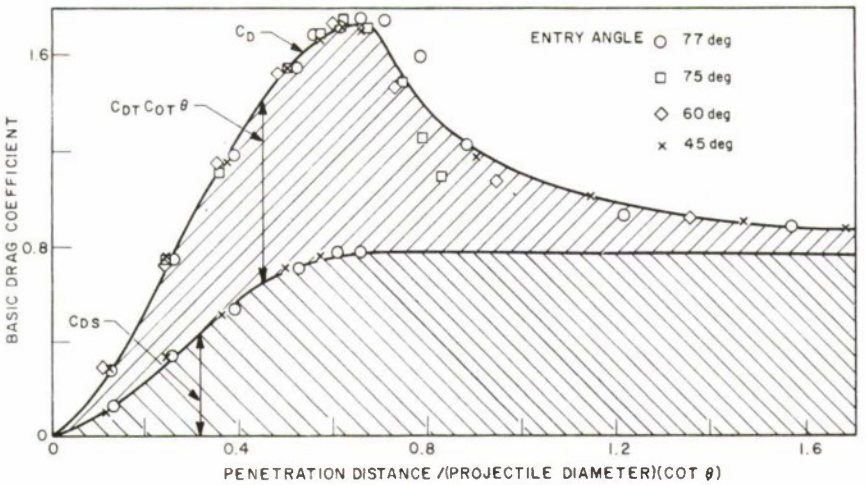

Figure B-1. Disk-cylinder steady-state and transient drag coefficients.

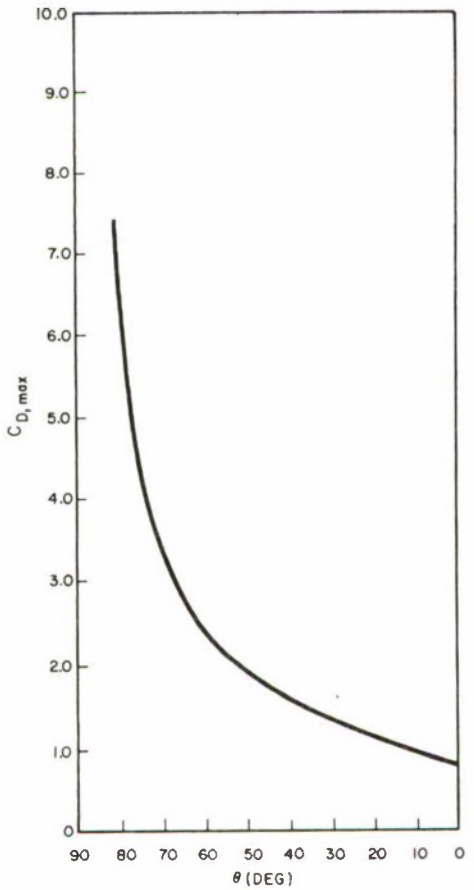

Figure B-2. Disk-cylinder maximum drag coefficient.

B-3.2 Vertical Entry of Axisymmetric Pointed Projectiles

The maximum drag coefficients of slender axisymmetric pointed projectiles depend little on entry angle. The maximum drag coefficients for blunt axisymmetric bodies, however, depend strongly on entry angle. Although the details of the phenomena are not understood in terms of C_{DT} and C_{DS}, drag-coefficient prediction techniques have been developed.* These techniques have been programmed for use with a timesharing type of computer. The coefficients are predicted by curve-fitting the experimental data given in Baldwin.[5] Cones, cusps, ogives, and paraboloids are approximated by a series of truncated cones; coefficients are computed for each element. The results of such a calculation agree with experimental data to about 20 percent for cusps, ogives, and paraboloids. Sample results obtained by use of these techniques are compared with the experiment in figure B-3 for a cusp and an ogive; the impact velocity in these examples is approximately 150 ft/s. As might be expected, the coefficients start at zero, maximize, and then decrease to a relatively steady value. Drag coefficient calculations for axisymmetric pointed bodies under specified conditions may be obtained from the authors. As an aid for estimation, however, figure B-4 shows the maximum and final C_{DS} for cones[5] and for tangent ogive.* The steady and maximum coefficients for bodies with sharp points do not differ.

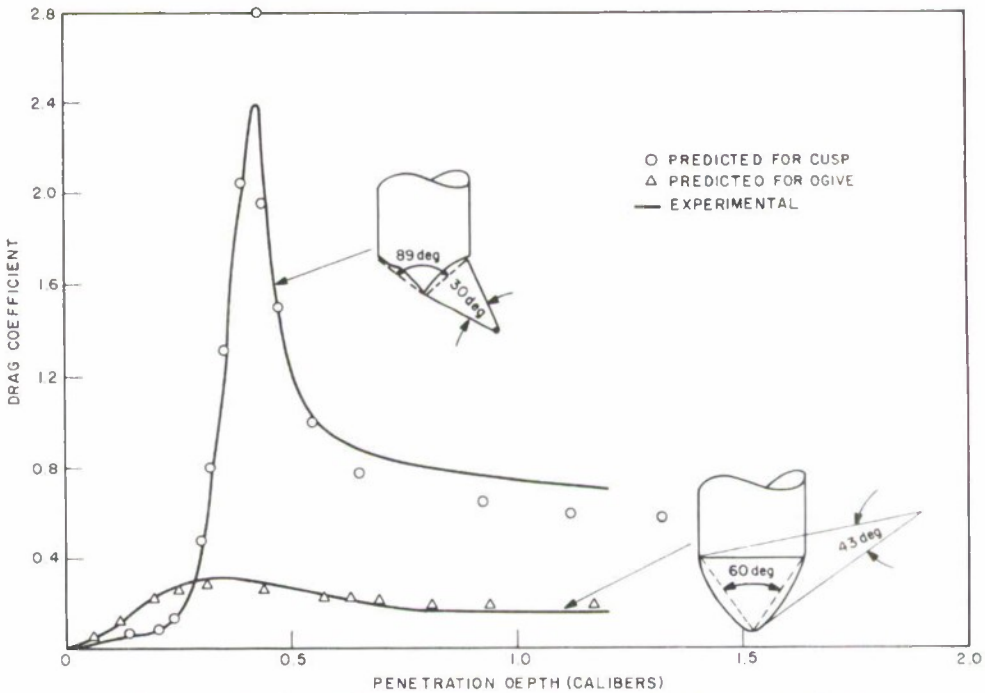

Figure B-3. Drag coefficients of typical cusp and ogive axisymmetric projectiles.

[5] *J. L. Baldwin, Vertical Water Entry of Cones, US Naval Ordnance Laboratory TR-71-25 (1971).*

**J. L. Baldwin, NOL, unpublished data.*

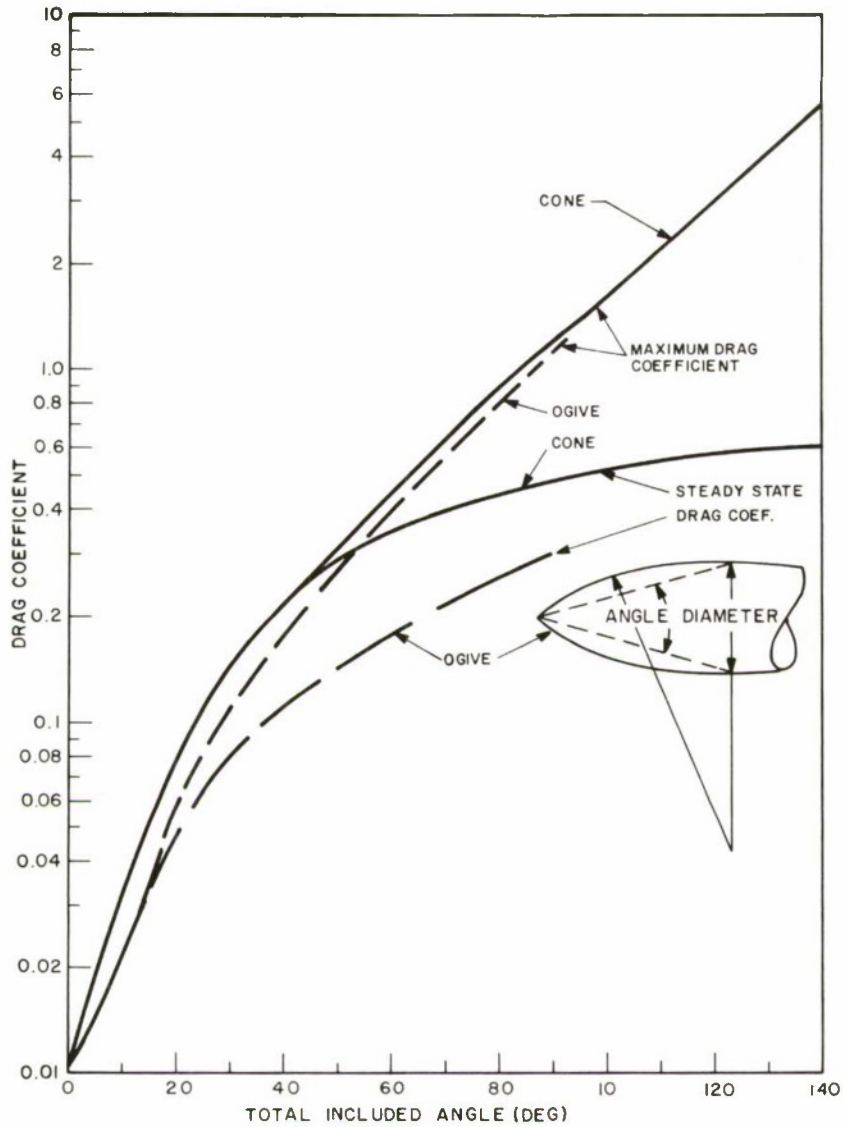

Figure B-4. Cone and ogive maximum and steady-state drag coefficients.

B-3.3 Drag Coefficients Due to Wave Phenomena

Wave phenomena have a significant effect on drag during high-velocity impacts. They are significant also when blunt-nosed bodies impact water normally at or near normal angles. One-dimensional theory predicts that the pressure behind such a wave is

$$P = \rho c u \ . \qquad \text{(B-7)}$$

Experimental results* indicate that the actual pressure achieved is 85 percent of the theoretical value. Thus,

$$F_D = PA = 0.85\ \rho cuA = 0.5\ \rho C_D A u^2 \qquad \text{(B-8)}$$

yielding as an equivalent drag coefficient

$$C_D = 1.7\ \frac{c}{u}\ . \qquad \text{(B-9)}$$

This wave-induced force lasts for microseconds. Its effect on drag, however, is longer lasting, since the water set in motion by the initial impact continues to interact with the projectile. The wave-induced drag coefficient should be superimposed on the results of other calculations in applicable situations.

As an example of the calculation of a wave-induced drag coefficient, a blunt-nosed projectile impacts water at 1000 ft/s. The u = 1000 ft/s, and c = 5000 ft/s. Equation (B-9) then yields

$$C_D = 8.5\ .$$

Equating this drag coefficient to equation (B-5) yields

$$\theta = 83.1 \text{ deg.}$$

This may be interpreted as meaning that 8.5 is the maximum possible drag coefficient for a body impacting water at 1000 ft/s at an angle between 90 and 83.1 deg.

B-3.4 Pressure-Actuated Fuze Drag Coefficients

These drag-coefficient discussions describe the deceleration of the entire projectile. They therefore apply to analyses of inertially actuated fuzes. Many fuzes, however, function because pressure is applied directly to the actuating element. Unfortunately for the sake of analysis, the pressure distribution around an impacting body is extremely complicated, particularly at high velocities. Estimates can be made by use of the drag-coefficient information already presented to calculate the forces acting on the body and then to divide these forces by the appropriate areas. These estimates should be used with caution.

Initial phenomena affecting pressure-actuated systems can be estimated somewhat. The mass of water in contact with the actuating mechanism is assumed to remain constant. The actual amount of water varies, since new water comes in to replace the water that is leaving.

R. Wasser, NOL, unpublished data.

As overall effect, this mass of water momentarily remains constant. Under these circumstances, the impulse transmitted to the actuating element is

$$I = \int_0^t F_D dt = \Delta(mu). \tag{B-10}$$

This discussion is restricted to disk-cylinder projectiles. The variables in the calculation can then be changed to a dimensionless distance where

$$\bar{S} = \left(\frac{S}{D}\right) \tan \theta$$

$$d\bar{S} = \frac{\tan \theta}{D} \, ds \tag{B-11}$$

$$dt = \frac{ds}{u} = \frac{D}{u \tan \theta} \, d\bar{S}. \tag{B-12}$$

From the data of figure B-1,

$$C_{DT} = f(\bar{S}) \tan \theta$$

$$\bar{S} \leq 0.61: \; C_{DS} = 0.85 \, f(\bar{S})$$

$$\bar{S} > 0.61: \; C_{DS} = 0.79.$$

Substituting into equation (B-10),

$$I = \frac{1}{2} Au^2 \rho \int_o^t (C_{DT} + C_{DS}) \, dt \tag{B-13}$$

$$= \frac{1}{2} Au^2 \rho \left[\int_o^{\bar{S}} f(\bar{S}) \, \frac{D}{U} \, d\bar{S} + \int_o^{0.61} \frac{0.85 \, f(\bar{S}) D}{u \tan \theta} \, d\bar{S} + \int_{-0.61}^{\bar{S}} \frac{0.79 \, D}{u \tan \theta} \, d\bar{S} \right]$$

$$= \frac{1}{2} \rho u \left(\frac{\pi}{4}\right) D^3 \left[\int_o^{\bar{S}} f(\bar{S}) d\bar{S} + \int_o^{0.61} \frac{0.85 \, f(\bar{S})}{\tan \theta} \, d\bar{S} + \int_{0.61}^{\bar{S}} \frac{0.79}{\tan \theta} \, d\bar{S} \right].$$

The function $\int_0^{\bar{S}} f(\bar{S})\, d\bar{S}$ can be obtained from figure B-1 by numerical integration. The result is shown in figure B-5.

To estimate the effects of nearly vertical impacts, consider the impulse caused by the C_{DT} term:

$$I_{DT} = \frac{1}{2} \rho \frac{\pi}{4} D^3 u \int_0^{\bar{S}} f(\bar{S}) d\bar{S} \ . \qquad \text{(B-14)}$$

The asymptotic nature of figure B-5 implies that $f(\bar{S})$ can be neglected for $S > 1.7$. The maximum value of $\int_0^{\bar{S}} f(S) dS$ is then 0.66. Thus,

$$I_{DT'max} = \left(\frac{1}{2} \rho \frac{\pi}{4} D^3 u\right) 0.66 \qquad \text{(B-15)}$$

$$= 0.502\, D^3 u \text{ (D in feet, u in feet per second)}$$

$$I_{DT'max} = 2.9 \times 10^{-4}\, D^3 u \text{ (D in inches, u in feet per second).} \qquad \text{(B-16)}$$

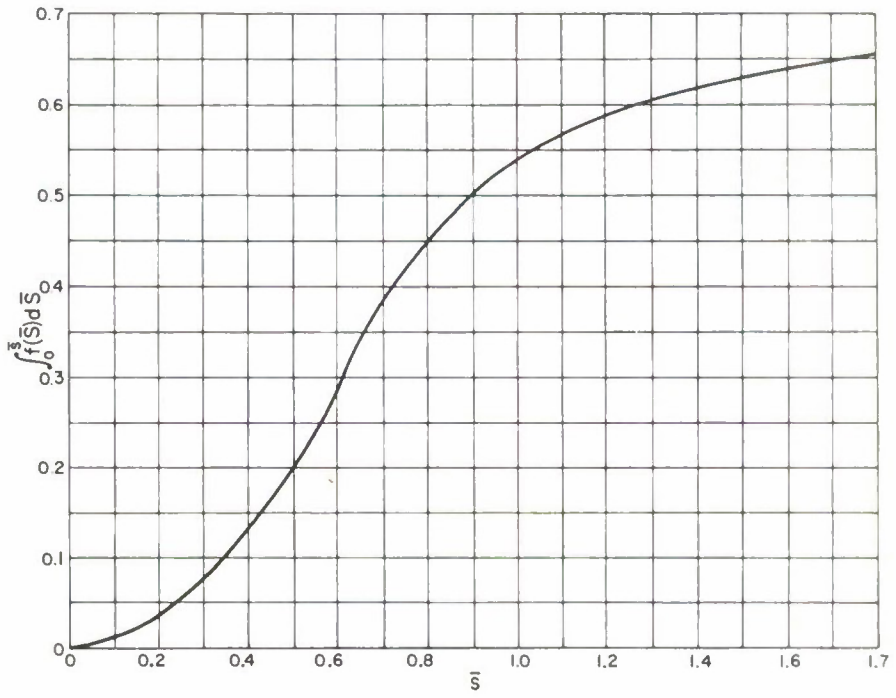

Figure B-5. Dimensionless distance function.

APPENDIX B

One can assume that the mass of the water in contact with the actuating element remains constant during the process and that the initial velocity of the element relative to the projectile is zero. Then equation (B-10) can become

$$I = mu \tag{B-17}$$

and, from equating equation (B-16) to equation (B-17) for the maximum case being considered,

$$m = 2.9\times10^{-4}\ D^3 \quad (m \text{ in slugs}). \tag{B-18}$$

B-4. EXAMPLES OF DRAG COEFFICIENT CALCULATIONS

Here are two examples of the use of drag coefficients to calculate the forces acting to retard the motion of a projectile.

B-4.1 Drag Acting on 155-mm Projectile

The drag acting on the XM613 155-mm projectile is calculated as an example. The appropriate dimensions of the shell are taken to be a projectile radius of 3.046 in., a cone angle of 22 deg, a swept angle of 13.45 deg, and a radius of curvature of 68.17 in. The fuze is assumed to be a continuation of the projectile surface. The fuze's flat nose has a radius of 0.276 in. The length of the nose is assumed to act as a flat-ended rod, shown schematically in figure B-6(a). The history of the drag coefficient when the projectile impacts normally at a velocity of 1000 ft/s is desired.

The drag coefficient for the fuze and projectile was calculated by the axisymmetric pointed body code, shown by the dashed line of figure B-6(b). To this is added the drag coefficient due to the impact of the flat nose. The initial flat-nose drag coefficient can be calculated by the wave theory, as was done in the example in section B-3.3. The value of 8.5 calculated there must be corrected for the appropriate reference area.

$$\text{Wave drag coefficient} = (8.5)\ \frac{(0.276^2\pi)}{(3.046^2\pi)} = 0.07\ .$$

The pressure wave propagates through the water spherically from the point of contact. A rarefaction wave is generated when this pressure wave passes the free edge of the projectile. The pressure at the contact point is assumed to be damped out by this rarefaction wave. With 5000 ft/s as the velocity of the waves in water, the time for a round trip of the waves across at a distance equal to twice the radius is calculated to be

$$t = \frac{(2.)(0.276)}{(12.)(5000.)} \sim 10^{-5}\ \text{s}.$$

A projectile traveling 1000 ft/s moves 0.01 ft in this time.

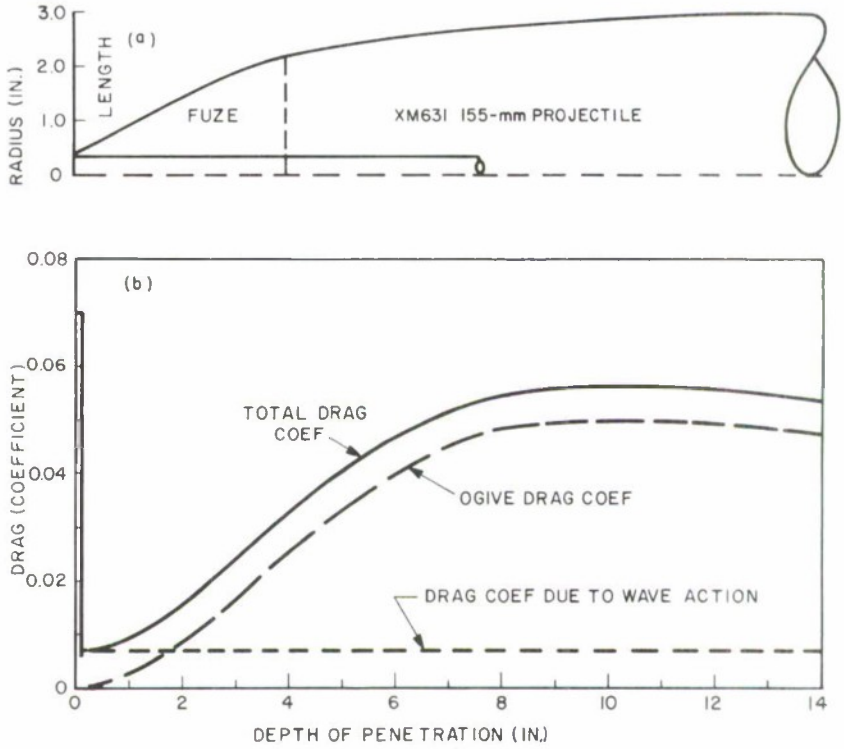

Figure B-6. Drag coefficient calculated for XM631, 155-mm projectile.

That flat-nose contribution to the C_{DS} for the projectile is given by the first term of equation (B-5). This drag coefficient, corrected for the reference area, is shown by the short-dashed line in figure (B-6(b)). The total drag coefficient, the sum of the wave and ogive components, also is shown in figure B-6(b).

Since the drag coefficient of 8.5 calculated for this example in section B-3.3 is the maximum that can be attained when the entry angle is between 90 and 83.1 deg, θ = 83.1 deg is used in equation (B-12) to calculate the maximum duration of the impulse.

B-4.2 Deceleration of Cannon-Launched Projectile

The deceleration acting on an 8-in.-diam, cannon-launched projectile can be estimated by the data already given. The projectile's ogive is 14 in. long and has a 45-in. radius of curvature. The tip of the nose is a 2-in.-diameter flat. The projectile weighs 250 lb. General estimates of the gravities acting on the projectile when it impacts water at 700 ft/s at a 45-deg angle are desired.

APPENDIX B

Both the ogive and the flat nose contribute to the projectile's drag. The ogive's geometry is such that its included angle is 31.8 deg. The data given in figure B-4 for an ogive with this angle indicate a maximum drag coefficient of 0.12 and a C_{DS} of 0.086. Since the drag coefficients of slender projectiles are independent of entry angle, these data will be used, even though they apply directly to normally entering projectiles.

The initial drag contribution of the flat nose can be obtained from figure B-2. The maximum drag coefficient due to the flat nose when it enters water at 45 deg is 1.71, which, when corrected for the reference area, is 0.11. The area-corrected flat-nose C_{DS} given by the first term of equation (B-5) is 0.049.

The drag forces acting on the projectile are

$$F_D = wG = \frac{1}{2} \rho A u^2 C_D$$

$$G = \frac{1}{2} \frac{A}{w} \rho u^2 C_D$$

$$= \frac{1}{2} \frac{62.4}{32.2} \frac{\pi}{12^2} \frac{(4.0)^2}{250} (700)^2 C_D$$

$$= 662.8 \, C_D .$$

The initial deceleration caused by the flat nose is

$$G = (662.8)(0.11) = 73 \text{ g}.$$

The maximum deceleration caused by the ogive is the sum of the disk-cylinder C_{DS} plus the ogive maximum:

$$G = (0.049 + 0.12)\ (662.8) = 112 \text{ g} .$$

The steady state drag deceleration is

$$G = (0.049 + 0.086)\ (662.8) = 89 \text{ g} .$$

B-5. SUMMARY AND DISCUSSION

The standard drag force equation can be used in water-impact problems with the greatest accuracy when the projectile is small and not very buoyant. The trajectory of the projectile is assumed to be stable within the water target. The error resulting from use of a constant velocity in the drag equation can be estimated by calculating the actual velocity change of the projectile after it travels the distance under consideration.

Drag coefficients for disk-cylinder projectiles entering at oblique angles are presented in detail in the text; detailed drag coefficients for axisymmetric pointed bodies entering normally are available from the authors. Data on the maximum and steady-state drag coefficients for these two geometries are specified in the report. Techniques of calculating the drag coefficients associated with wave phenomena and the impulse caused by the initial impact also are presented. Two examples of the use of these coefficients are presented.

Drag coefficients are area- and time-averaged quantities. The more general the use of a drag coefficient, the greater the error. However, the coefficients and entry conditions dealt with in this report apply significantly in much ordnance work and should yield relatively accurate estimates.

APPENDIX B

ABBREVIATIONS AND SYMBOLS

A	Projectile area
B	Buoyant forces
c	Velocity of sound in water
C_D	Total drag coefficient
C_{DS}	Steady state drag coefficient
C_{DT}	Transient component of drag coefficient
D	Projectile diameter
F	Generalized forcing function
F_D	Forces due to drag
G	Projectile deceleration divided by g
g	Acceleration due to gravity
I	Impulse
I_{DT}	Impulse caused by transient drag
M	Mass of projectile
m	Mass of water
P	Pressure in water
S	Penetration depth
$\bar{S}$	Dimensionless distance (eq 12)
t	Time
u	Projectile velocity
w	Projectile weight
θ	Entry angle of projectile, measured from the horizontal
ρ	Water density

SUBSCRIPTS

max	Maximum value
o	Initial value

APPENDIX C.--EXISTING MECHANICAL IMPACT SWITCH CONCEPTS

Point detonating (PD) fuzes are initiated by mechanical elements when they impact their target. Many PD fuzes are used by the US Army.[1]* Table C-I lists the design characteristics of each of these mechanical elements. Supplemental information was gathered from appropriate Technical Information Reports.[2] The table indicates that pressure-driven elements are the primary means by which these fuzes are activated; inertial elements, on the whole, provide delay functioning or graze functioning or insure that no live ammunition is on the battlefield after an encounter.

TABLE C-I. DESIGN CHARACTERISTICS OF IMPACT ELEMENTS USED IN POINT DETONATING FUZES PRESSURE ACTUATED SWITCH

Fuze	Deforms gilding metal support	Deforms elastic spring	Drives free-floating firing pin	Inertia drives detonator and firing pin together
M48A2 & A3	X			X
M51A4 & A5	X			X
M52		X		
M53A1	None			(Shear pin deformed)
M56			X	
M57	X			
M74			X	
M78 & A1	Unknown			X
M82		X		
M89	X			
M503, A1 & A2	X			X
M519		X		
M521	X			X
M524 series		X		X
M525 & A1		X		
M526 & A1		X		Unknown
M527, B1 & A1		X		Unknown
M535	X			X
M557	X			X
M572	X			X
XM593		X		X
MK27			X	
XM716		X		
XM717		X		
XM719		X		
XM720E1	X			X

*See Literature Cited for all references in appendix C (p. 44).

APPENDIX C

Pressure-driven PD fuzes use one of two basic elements to maintain the impact element in the nonfiring position--a plastically deforming cylinder or an elastically deforming helical spring. The elastic spring returns to equilibrium after the driving force is removed. This characteristic is an advantage if the fuze is to be used in a rainstorm, since plastic members cumulatively deform after a number of raindrop impacts. This deformation can be offset by making the crush strength of the material greater than the load applied by the raindrop impact, but doing so reduces the sensitivity of the fuze. The bias strength of an elastic member can be kept low, enhancing its impact sensitivity, if the length of travel of the switch's actuating member is greater than its expected displacement during an early impact.

The impact element design characteristics of a number of point-initiating (PI); mechanical time, super quick (MTSQ); and proximity fuzes are listed in table C-II. In the PI and MTSQ fuzes, the pressure-driven element appears to predominate; plastically deforming metal cylinders, fuze ogive, and piezoelectric crystals are used. The

TABLE C-II. IMPACT ELEMENT DESIGN CHARACTERISTICS FOR OTHER THAN PD FUZES

Fuze type	Firing pin	Fuze	Characteristic
Point initiating	Inertially driven	XM539E4	Electrical switches close, discharging capacitor
	Pressure driven	M90A1 XM579	Ogive impacts primer (for XM579, delay mode provided by inertially driven [spin decay] pin impinging on detonator)
		M509 M530 M371A1 XM559	Piezoelectric crystal deformation (for M530, graze backup provided by inertially driven pin impinging on detonator)
Mechanical time, super quick	Inertially driven	M502 M506 M518	No restraining element
	Pressure driven	M500 M501 M520 M548 M564	Pin held by gilding metal support
		M577	Pin held by honeycomb restraining element
Proximity	Inertially driven	M514 series M517 M532 M429 XM728 XM732 FMU-98	Spring-loaded beam
		598	Centrifugal force biased pin
	Pressure driven	M513 series M515 M516 series	Plastically deforming ogive closes electric contacts (for M515 and M516 series, inertially driven [spin decay] switch included in some models)

M577 fuze is different in using a honeycomb biasing element. Inertial elements are used with some of the pressure-driven elements as a delay or graze action unit. An example of the use of both of these switches together is the US Navy's "Redeye" fuze (not listed in table C-II). A crush switch sets off its shaped charge when it impacts a hard-skinned target, and an inertial switch sets off its explosive train when it impacts a soft target.

The need for very quick fuze response against thin-skinned airborne targets has led to the use of several MTSQ fuzes that are not biased at all. But they should not be used in heavy rainstorms.[1] Early proximity-fuze designs used plastically deforming ogives as switch elements to back up the electronic sensor. The sensitivity of such devices to the angle of impact led to the development of an inertially driven, spring-loaded switch.[3,4]

Additionally, patents and published reports inform about the state of the art of impact fuzing. Table C-III lists US patents dealing with impact switches. Most patents listed are for inertially driven devices. Thus centrifugal force drives a cantilever beam (No. 2,685,008), an oil-damped slider (No. 2,712,791), a mass biased by a leaf spring (No. 2,900,909), a beam with means of compensating for various spin rates (No. 3,181,466), and two spring-biased masses acting in tandem (No. 3,286,057). Means of increasing the sensitivity of an inertial switch have been seriously considered. Patented concepts include a beam tilted by a ball (No. 2,977,881), a beam tilted by its dumbbell-shaped end (No. 3,718,093), a ball-cylinder combination (No. 3,511,184), and a diaphragm that is ruptured by an increase in fluid pressure (No. 3,453,406).

Other concepts have been used to enhance the sensitivity of inertial impact elements. Thus, the mechanical advantage offered by a ramp has been used in the Picatinny Arsenal version of the high-performance fuze,[5] the force acting on the detonator has been increased by having it and various parts of the fuze move onto the firing pin,[6,7] and the deceleration of a 40-mm projectile during impact has been increased by its nose being blunted.[8] The graze sensitivity of an impact fuze has been increased by use of two orthogonally mounted switches (No. 3,410,215), two orthogonally mounted cantilever beams (No. 3,492,450), a number of shaped leaves (No. 2,934,018), a ball and plate (No. 3,158,705), and the inertia of a rotating ring (No. 3,264,995). A design using the inertia of a rotating ring mounted on a shaft has been studied for use in British fuzes.[9] Patent No. 3,054,870 describes a switch that discriminates between water and solid deceleration. A design aimed at enhancing omnidirectional sensitivity uses a number of balls biased by springs (No. 2,741,674). This switch has been incorporated into a number of fuzes.[10] A specially designed element is claimed to offset the variable bias as the ball moves along the biasing beams (No. 3,156,794).

APPENDIX C

TABLE C-III. SELECTED IMPACT ELEMENT PATENTS

Patent No.	Date filed	Author	Title	Assigned to
2,685,008	Sep 1943	T. H. Darnell	Centrifugal Force Operated Switch	US Navy
2,712,791	Jul 1942	R. M. Bleakney et al	Switch	US Navy
2,741,674	Sep 1954	E. D. Richard	Impact Switch	US Army
2,796,025	Apr 1955	H. E. Ruppel	Detonating Device	Magnavox
2,856,853	Oct 1956	R. P. McGinnis	Impact Switch	US Army
2,887,056	Jan 1956	J. Perret	Contactor Device for Projectile	Motha ene Liechtenstein
2,900,909	Aug 1943	J. Jordan	Centrifugal Switch	US Navy
2,931,301	May 1956	K. Helm et al	Ballistic Missile Fuze	Bofors, Sweden
2,934,018	Aug 1958	F. Seavey	Fuze	Olin Mathieson
2,977,881	Feb 1955	C. Piper	Trigger Releasing Device	Magnavox
3,054,870	Jun 1958	B. Waggoner	Variable Sensitivity Inertial Switch	US Navy
3,111,089	Nov 1960	H. Dodson	Frangible Firing Device	US Army
3,135,206	Sep 1957	K. Helm et al	Fuze for Projectiles	Bofors, Sweden
3,156,794	Dec 1962	I. Vold	Omnidirectional Impact Switch	Honeywell
3,158,705	Dec 1962	R. Bliss	Combination Graze and Impact Switch	US Army
3,181,466	Feb 1957	N. Czajkowski	Spin Compensating Switch	US Navy
3,190,222	Jul 1962	G. Holmstron	Impact Sensitive Top Fuze	Forsvarets Fab., Sweden
3,196,794	Jun 1959	R. Meade	Piezoelectric Fuze Drive	US Navy
3,264,995	May 1964	T. Libbey et al	Mechanical Fuze Operable on Grazing Impact	AVCO
3,286,057	May 1964	P. Krupen	Centrifugal Switch	US Army
3,339,090	Oct 1963	H. Jaffe et al	Piezoelectric Impact Fuze	US Army
3,351,018	Mar 1965	H. Bedall	Percussion Fuze	Diehl, Germany
3,356,026	Nov 1964	J. Lubig	Piezoelectric Igniter for Projectiles	Nobel, Germany
3,359,901	Jul 1965	H. Bedall	Explosive Shell Having Contact Fuze	Diehl, Germany
3,359,904	Jul 1966	F. Nerheim	Piezoelectric Projectile Fuze	Honeywell
3,372,642	Aug 1964	J. Brothers	Internal Firing Switch	US Army
3,410,215	Jun 1967	R. Apotheloz	Impact Fuze	Oerlikon, Switzerland

TABLE C-III. SELECTED IMPACT ELEMENTS PATENTS (CONT'D)

Patent No.	Date filed	Author	Title	Assigned to
3,417,699	May 1956	W. Piper	Contact Fuze	US Army
3,440,961	Nov 1966	E. Fohrmann et al	Contact fuzing System	US Army
3,453,406	Sep 1967	K. Pope	Impact Arming and Tamper Switch	UMC Industries
3,468,256	Dec 1967	J. Vanover	Impact Fuze Assembly	US Navy
3,492,450	Jan 1969	B. Stockdale et al	Inertia Switch	AVCO
3,511,184	Apr 1968	R. Bowers	Inertia Impact Firing Mechanism	AVCO
3,718,093	Apr 1971	F. Milanowski	Firing Pin Assembly	US Army
3,098,163	Jul 1960	R. Bliss	Inertial Energy Generator Storage System	Magnavox

Several pressure-actuated fuze concepts have been patented. These include elements with shear noses (No. 2,931,301), shoulders (No. 3,351,018 and 3,359,901), crush walls (No. 3,111,089), internal liners (No. 3,372,642) and caps (No. 3,468,256). The graze sensitivity of a pressure-actuated round has been addressed by making the entire ogive part of the sensing element. The problem of prematurely denting the outer sensing element during shipping has been met by making the outer wall elastic and using a grid of wires or a metallic coating on this wall (No. 2,887,056). Another modification is to put the primary explosive in the gap between two surfaces and to activate this explosive during impact by pinching it (No. 3,190,222). An impact switch[11] uses a pressure-actuated element mounted on a probe that is extended in front of the projectile while in flight.

One switch used in a US fuze was specifically designed to function using the stress waves generated during an impact. This design uses a ball sitting on three legs. Electronic logic causes the fuze to function when the ball leaves two of the legs. This switch and a number of others use stress waves.[3,4,12] Patents No. 3,196,794, 3,417,699, and 3,440,961 similarly include wave-actuated elements.

Several impact switches have been designed using the previously discussed elements, which generate their own electrical power. Thus, many US Army projectiles used against tanks incorporate piezoelectric crystals that are crushed on impact with the target; the resulting charge is passed through a carbon-bridge detonator. On the other hand, the Soviet RPG-7 fuze apparently breaks down the dielectric strength of an explosive, using the potential generated by an impacted piezoelectric crystal.[13] Patents No. 3,339,090 and 3,356,026 describe inertially driven piezoelectric fuze elements. The most efficient means of using piezoelectric generated power has been studied.[11]

Some fuzes have been designed that inertially generate charge upon setback; they use a cantilever beam as a mechanical diode, store the generated charge in the hermetically sealed crystal itself, and discharge into the detonator on impact. Patent No. 3,098,163 presents the principle behind the energy generator. The devices have been designed, tested, and subsequently investigated.[14-19]

APPENDIX C

Piezoelectric crystals used as signal sources rather than as sources of energy for detonators (No. 3,359,904) are apparently used in the AVCO version of the high performance fuze[20] and in the probe sensor used in the US Air Force Pave Way bomb.[21]

Self-powered impact switches also use magnets. Patent No. 2,977,881 describes a magnet that, when released by the impact forces, is driven through a coil. In a similar fashion, inertial forces generated during impact pull the magnet away from the coil in the US Navy's MK191 fuze. In both cases, the power generated sets off an electrical detonator. The switch described in patent No. 2,796,025 functions when it penetrates the metal skin of a projectile.

LITERATURE CITED

(1) Artillery Ammunition, US Army Technical Manual 9-1300-203 (1967).

(2) Subject Index of Technical Information Reports, US Army Materiel Command Technical Information Report AMC-B-6 (1969).

(3) C. Conlon and A. Johnson, Advanced Contact Fuze Sensor (U), AVCO Systems Division Technical Report SAMSO-TR-71-205 (1971). (SECRET-RESTRICTED DATA).

(4) B. C. Ruddy, Elastic Wave Surface Impact Fuze (U), General Electric Missile and Space Vehicle Dept. Report 61SD133 (1961). (CONFIDENTIAL)

(5) Picatinny Arsenal Concept Formulation of a High Performance Mechanical Artillery Point Detonating Fuze, vol. I, II, Fuze R&D Laboratory, Ammunition Engineering Directorate, Picatinny Arsenal (1971).

(6) J. P. Hunt, Development of an Impact Initiating Safety Adaptor for the M514A1E1 VT Fuze Product Improvement Program, Frankford Arsenal Report R-1958 (1970).

(7) W. George, Demonstration of the Feasibility of Adapting the M514A1E4/M572 Fuze S&A Module to the Sliding Module S&A Device for the XM587E2/XM734 Electronic Time Fuze, Honeywell, Inc., Report HDL-0039-1 (1972).

(8) R. Sward and H. Seavey, Product Improvement of the M551 Fuze, Amron-Orlando Summary Report on Contract DAA21-70-C-0185 (1970).

(9) Operating Characteristics of Gyroscopic Switch Type 3591, Inertia Switch [United Kingdom] Limited Report (1970).

(10) D. Miller, Fuze PD XM538 and XM538E1 (U), Eureka Williams Company Final Report on Contract DA-49-186-502-ORD(P)799 (1963). (CONFIDENTIAL)

(11) J. J. Furlani, Feasibility Study of Extensible Probe for Mortar Shell, Diamond Ordnance Fuze Laboratories Report TR-320 (1956).

LITERATURE CITED (CONT'D)

(12) W. Todd and R. Haskell, Guided Missile Contact Fuzing (U), Rheem Manufacturing Company, Summary Report on Contract N123 (62738) 18681A (1960). (CONFIDENTIAL)

(13) H. J. Davis and J. Beard, Exploitation Report--Fuze, PIBD, Model VP, Soviet, MCN-29403 (U), Foreign Science and Technology Center Report FSTC-CR-20-2-70 (1969). (CONFIDENTIAL)

(14) D. A. Bednar, Development, Fabrication and Testing of Fuze PIBD, XM569 and Associated Assemblies (U), Magnavox Company Progress Report on Contract DAA2 8-017-AMC-1115(A) (1964). (CONFIDENTIAL)

(15) D. A. Bednar, Fuze PIBD, T370 Series (U), Magnavox Company Final Report on Contract DA-11-022-ORD-3454 (1964). (SECRET)

(16) M. Rosenblatt and N. Louie, Analysis of the Components of the XM22 Contact Power Supply (U), Shock Hydrodynamics, Inc., Final Report on Contract DAAA 21-70-C-0262 (1970). (CONFIDENTIAL)

(17) L. Watermier and R. Eichelberger, ARCD Investigation of XM409E4 Modified 152mm HEAT Round, Aberdeen Research and Development Center TR-7 (1970).

(18) E. Bisson, Graze Improvement Program on the 152 MM XM409E5 HEAT-T-MP Cartridge (U), Picatinny Arsenal Report TR-42606 (1971).(CONF)

(19) H. Gay and E. Wineholt, The In-Bore Motion of a Cantilever Beam Mounted in an Artillery Projectile, Ballistic Research Laboratories Memorandum Report 2150 (1972).

(20) High Performance Point Detonating Fuze Concept Formulation, AVCO Corporation Interim Report on Contract DAAA 21-70-C-0040 (1970).

(21) K. Wilkes, Evaluation of Piezoelectric Fuzing System in Laser Guided MK82 Bombs (U), Air Development Test Command, Eglin AFB, TR-71-146 (1971). (CONFIDENTIAL)

APPENDIX D.--SHOCK WAVE ANALYSIS

When an impacting body strikes a target at rest, the front of the projectile slows down, and the front of the target begins to move. In both bodies, the density near the interface increases to compensate for the change in velocity of the material. Because the bodies are in contact, the physics of the situation requires that (1) the particle velocity be the same on each side of the interface and (2) the pressure be the same on each side of the interface. The problem is to predict the pressure and particle velocity at impact. It is assumed that the impact is normal and that there is no cushioning material, such as air, between the impacting surfaces.

Zones of high pressure and high density spread in both directions from the interface of the impact. The leading edge of each zone, a shock wave, travels at a speed determined by the properties of the medium. It can be shown[1] from conservation of mass and momentum that the shock wave velocity, U, the particle velocity, u, and the pressure behind the shock wave, P, are related by the following equations:

$$P = \rho_0 u U \tag{D-1}$$

and

$$\rho_0 U = \rho (U-u) \tag{D-2}$$

where ρ_0 and ρ are the densities in front of and behind the shock wave, respectively.

A third relation, called the dynamic equation of state or the Rankine-Hugoniot relation, gives the density of a medium as a function of its pressure. This function is frequently written in the form of the polynomial

$$P = C\mu + D\mu^2 + S\mu^2 \tag{D-3}$$

where $\mu \equiv \frac{\rho}{\rho_0} - 1$.

Experimental values of C, D, and S are available for many materials.

For solving the impact problem, it is convenient to have a relation between pressure and particle velocity (P versus U). The intersection of two P-U curves shows the possible values of P and U that two materials can share; thus, these values occur at impact.

A set of such curves is shown in figure D-1. For example, consider the impact of an aluminum projectile, traveling at 200 ft/s, with water that is at rest. Before collision, the aluminum has a particle

[1] *M. H. Rice et al, Compression of Solids by Strong Shock Waves, Solid State Physics 6, Academic Press, New York (1958).*

APPENDIX D

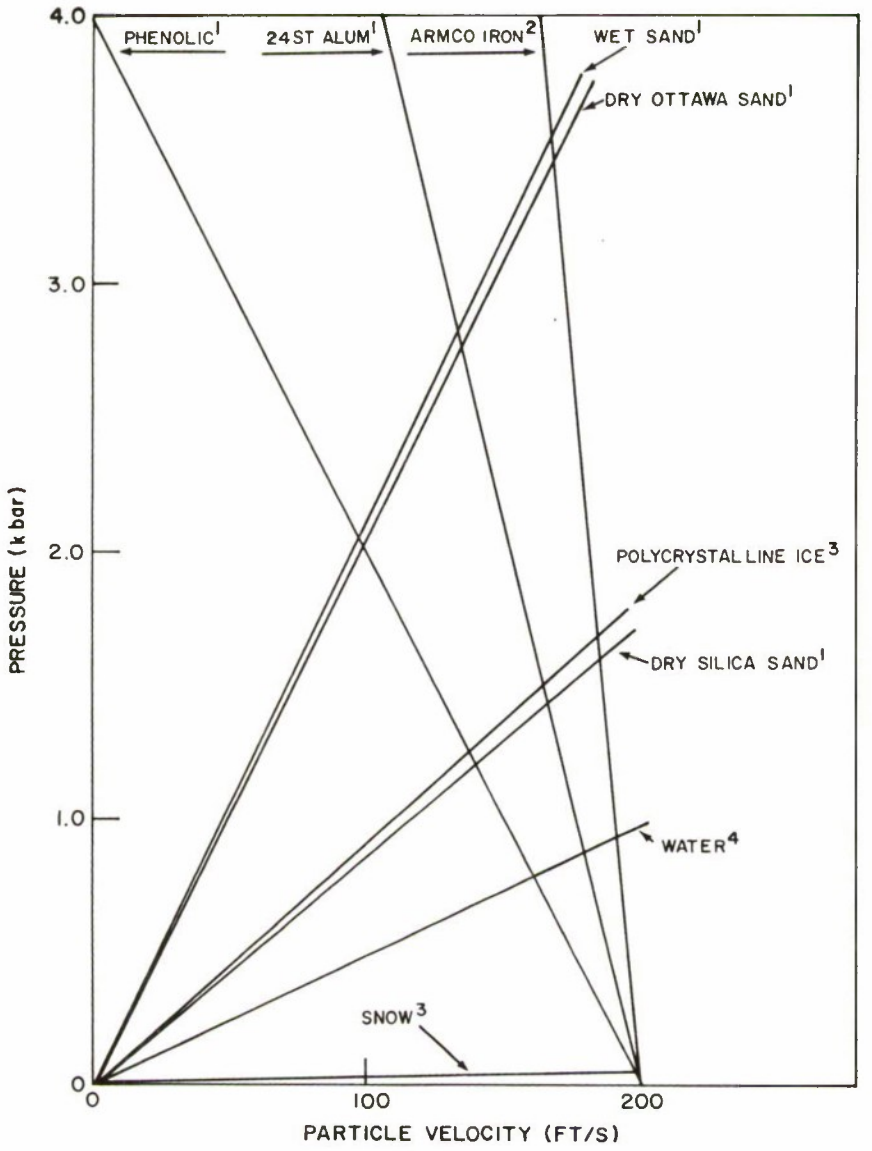

[1]*J. S. Rinehart, US Naval Ordnance Test Station TP-3798 (1965).*

[2]*J. W. Taylor and M. H. Rice, J. Appl. Phys., 24 (1963), 364.*

[3]*J. D. Anderson, Stanford Report CRREL 257 (1968).*

[4]*W. Walker, private communication.*

Figure D-1. Shock wave properties occurring during different projectile-target impacts (impact velocity 200 ft/s).

velocity of 200 ft/s and zero pressure, so the curve must pass through these coordinates. The curve for water must pass through zero velocity and zero pressure. At impact, as shown in figure D-1, the velocity must be U = 180 ft/s and pressure must be P = 0.87 kbar in both materials. Thus, the front of the aluminum projectile compresses immediately, and the velocity of the front end slows from 200 to 180 ft/s at impact Also, the water near the projectile has its velocity changed from 0 to 180 ft/s. A pressure wave sweeps through the projectile, reflects from the free surface, and returns to the interface, at which time a second change in velocity occurs. In this way the projectile is slowed in steps until it finally comes to rest.

The curves in figure D-1 were obtained from equations (D-1) to (D-3). Elimination of U from equations (D-1) and (D-2) gives

$$u^2 = \frac{(\rho-\rho_0)}{(\rho\rho_0)} P. \qquad (D-4)$$

Since P is a known function of ρ, one can assume a value of ρ and calculate P from equation (D-3) and U from equation (D-5). If they are calculated for a set of values of ρ, one can plot P versus U.

If one also wants to know the velocity of the shock wave, one can obtain U from

$$U = \frac{P}{\rho u} \qquad (D-5)$$

where P and u are known. However, for the low pressures that are characteristic of impact at velocities of a few hundred feet per second, the shock-wave velocity is always approximately (but slightly above) the velocity of sound in the medium.

For water, the Tait equation with parameters used at the Naval Surface Weapons Center, White Oak, MD, is

$$P = 3.05\left[\left(\frac{\rho}{\rho_0}\right)^{7.15} - 1.0\right] \text{kbars}$$

where ρ = density, and ρ_0 = density at zero pressure. This equation was used to generate data fitted to equation (D-3). The resulting coefficients were

$$C = 21.86$$

$$D = 64.70$$

$$S = 146.6 \ .$$

APPENDIX E.--ELECTRONIC IMPACT SWITCH

An ideal impact switch would have the sensitivity and fast response time of a pressure-activated device and the impact angle independence and ease of installation within a fuze structure of an inertial device. The extreme variability of the environment and of target and projectile parameters suggests that it will be difficult to fulfill all of these goals with a single device. The many impact switch designs that have been developed and tested over the years further suggest that it will be difficult to advance the state of the art towards the goal of an optimum impact switch using a simple mechanical design.

Figure E-1 is a schematic diagram of a transducer and electronic circuit designed to fulfill these goals. A ball rests on a ring of piezoelectric material. The piezoelectric crystal is polled as shown. Longitudinal or transverse inertial forces cause the ball to press against the ring and generate a voltage. Different settings in the electronic circuit set manually before firing are provided to allow for extreme sensitivity, for elimination of short-duration transients such as occur when a projectile flies through foliage and rainfields, or for delayed functioning within the target. The threshold at which the circuit functions is low, thus permitting quick achievement of the triggering voltage and allowing the fuze to function shortly after impact.

A longitudinal force acting on the fuze causes the ball to press on the crystal. The mechanical stop prohibits damage to the crystal when the fuze is inadvertently dropped. The stress created in the crystal by this force generates a voltage. In a similar fashion, transverse

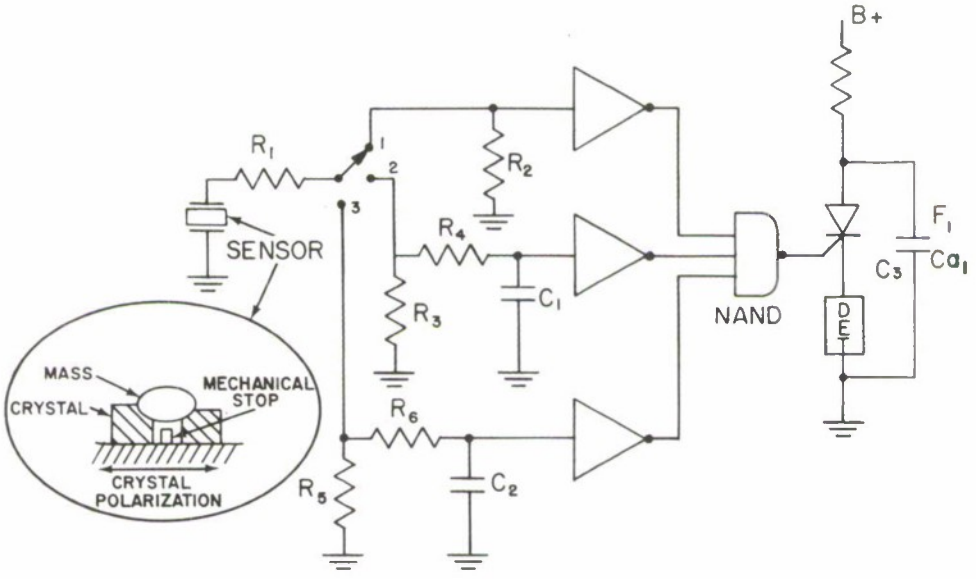

Figure E-1. Electronic impact switch.

forces generate voltages. Polling the crystal as shown causes larger voltages to be generated by the relatively weak transverse forces than would be generated by comparable longitudinal forces. Proper design of the transducer should permit the same unit to be used for longitudinal and transverse forces with a single threshold level used in the electronic circuitry.

Referring to figure E-1, in switch position 1, the resistors R_1 and R_2 divide the crystal's output down to the 5 to 15 V needed to operate the CMOS threshold detectors. This corresponds to the "superquick" mode of action, since there is no delay.

In switch position 2, resistors R_1 and R_3 provide the necessary attenuation, while R_4 and C_1 provide a time delay to avoid firing on short-duration pulses. The attenuation provided by the R_1 and R_2 combination is greater than that occurring in switch position 1. Position 2 thus provides a relatively sensitive impact function that can nevertheless be used in rainstorms.

In switch position 3, resistors R_1 and R_5 provide relatively large attenuation, while R_6 and C_2 provide a relatively long delay after impact. This corresponds to a delay-mode function.

The NAND gate is connected directly to the firing circuit. If any of the inverter outputs go to "low," the NAND gate fires the SCR.

DISTRIBUTION

DEFENSE DOCUMENTATION CENTER
CAMERON STATION, BLDG 5
ALEXANDRIA, VA 22314
ATTN DDC-TCA (12 COPIES)

DIRECTOR
DEFENSE ADVANCED RESEARCH PROJECTS AGENCY
ARCHITECT BUILDING
1400 WILSON BLVD
ARLINGTON, VA 22209
ATTN DIR, TACTICAL TECHNOLOGY
ATTN DIR, TECH INFO

DIRECTOR OF DEFENSE RES & ENGINEERING
WASHINGTON, DC 20310
ATTN ASST DIR (RSCH & ADV TECH)
ATTN ASST DIR (TAC WARFARE)

OFFICE, CHIEF OF RESEARCH, DEVELOPMENT & ACQUISITION
DEPARTMENT OF THE ARMY
WASHINGTON, D.C. 20310
ATTN DAMA-ART, ADVANCED SYSTEMS
ATTN DAMA-DDC, COMBAT MATERIEL DIV

COMMANDER
US ARMY MATERIEL DEVELOPMENT & READINESS COMMAND
5001 EISENHOWER AVENUE
ALEXANDRIA, VA 22333
ATTN DRCRD, DIR RES, DEV & ENGR
ATTN DRCRD-E, ENGINEERING DIV
ATTN DRCRD-P, PLANS & PROGRAMS DIV
ATTN DRCRD-W, WEAPONS/MUNITIONS SYSTEMS DIVISION

COMMANDER
US TEST & EVALUATION COMMAND
ABERDEEN PROVING GROUND, MD 21005
ATTN AMSTE-FA, FIELD ARTILLERY TEST DIR
ATTN AMSTE-AD-T, TECH INFO CENTER

COMMANDER
USA ABERDEEN PROVING GROUND
ABERDEEN PROVING GROUND, MD 21005
ATTN STEAP-MT-A, ARTILLERY DIV
ATTN STEAP-MT-G, L HEPPNER
ATTN J. FASIG

COMMANDER
USA MISSILE COMMAND
REDSTONE ARSENAL, AL 35809
ATTN AMSMI-R, MISSILE RD&E LAB
ATTN TECHNICAL LIBRARY
ATTN AMCPM-LSX, LAND COMBAT SPT
ATTN AMCPM-RK, 2.75" ROCKET SYS

COMMANDER
YUMA PROVING GROUND
YUMA, AZ 85364
ATTN STEYP-ADT, TECH LIB

COMMANDER
JEFFERSON PROVING GROUND
MADISON, IN 47250
ATTN M. SAVAGE

COMMANDER
USA ELECTRONICS COMMAND
FORT MONMOUTH, NJ 07703
ATTN AMSEL, DIRECTOR, LABORATORIES
ATTN AMSEL-RD, DIRECTOR RD&E

COMMANDER
USA ARMAMENTS COMMAND
ROCK ISLAND, IL 61201
ATTN AMSAR-SC, CHIEF SCIENTIST
ATTN AMSAR-ASF, FUZE DIV
ATTN AMSAR-RDF, SYS DEV DIV-FUZES
ATTN AMSAR-RDG, M RYAN
ATTN AMSAR-CAWS

COMMANDER
WATERVLIET ARSENAL
WATERVLIET, NY 12189
ATTN SARWV-RDD, MR RUMMEL
ATTN SARWV-RDD-SP, SPECIAL PROJECTS
ATTN SARWV-RDT-L, DOCUMENTS LIBRARY

COMMANDER
PICATINNY ARSENAL
DOVER, NJ 07801
ATTN SARPA-AD, AMMUNITION DEV & ENGINEERING DIR
ATTN SARPA-AD, AMMUNITION DEV DIV
ATTN SARPA-AD, FUZE DEV & ENGR DIV
ATTN SARPA-FR, FELTMAN RESEARCH LAB
ATTN SARPA-TS-T-S, TECHNICAL LIBRARY
ATTN AMCPM-SA, SELECTED AMMO

COMMANDER
FRANKFORD ARSENAL
BRIDGE & TACONY STREETS
PHILADELPHIA, PA 19137
ATTN J6000, ARTY AMMO COMPONENTS DIV
ATTN L1000, PITMAN-DUNN LABORATORY
ATTN L4000, SC AMMO RESEARCH DIV
ATTN K1000, TECHNICAL LIBRARY

COMMANDER
ARMY MATERIALS & MECHANICS RESEARCH CENTER
WATERTOWN, MA 02172
ATTN TECH INFO CENTER

DIRECTOR
USA MATERIEL SYSTEMS ANALYSIS AGENCY
ABERDEEN PROVING GROUND, MD 21005
ATTN AMXSY-D, DR J SPERAZZA
ATTN AMXSY-RW, WEAPONS & MUNITIONS
ATTN AMXSY-GI, INFANTRY WEAPONS

DIRECTOR
USA ADVANCED MATERIEL CONCEPTS AGENCY
2461 EISENHOWER AVENUE
ALEXANDRIA, VA 22314
ATTN FUTURE TRENDS DIR

COMMANDING OFFICER
USA FOREIGN SCIENCE & TECHNOLOGY CENTER
FEDERAL OFFICE BUILDING
220 7TH STREET, NE
CHARLOTTESVILLE, VA 22901
ATTN AMXST-CM, COMBAT MATERIEL DIV
ATTN AMXST-RD, RES & DOCUMENT DIV
ATTN AMXST-FA2, MR BOLENDORF

COMMANDER
USA MISSILE & MUNITIONS
CENTER AND SCHOOL
REDSTONE ARSENAL, AL 35809
ATTN ATSK-CTD-F

COMMANDER
US ARMY RESEARCH OFFICE (DURHAM)
PO BOX 12211
RESEARCH TRIANGLE PARK, NC 27709
ATTN ENGR SCI DIV, DR S KUMAR

COMMANDER
NAVAL SURFACE WEAPONS CENTER
WHITE OAK, MD 20910
ATTN CODE 730, LIBRARY DIVISION
ATTN CODE 043, PROJ MGR, FUZES
ATTN 1-315, TECH LIBRARY
ATTN CODE 412, MECHANISMS DIVISION
ATTN CODE 322 HYDRO & MECH DIV

COMMANDER
NAVAL SURFACE WEAPONS CENTER
DAHLGREN, VA 22448
ATTN TECHNICAL LIBRARY
ATTN DT 54, DR G MOORE

COMMANDER
NAVAL WEAPONS CENTER
CHINA LAKE, CA 93555
ATTN CODE 454, APPL RSCH & PROC DIV
ATTN CODE 39, WEAPONS DEPT
ATTN CODE 455, ENGR DIV
ATTN CODE 553, PROD DES DIV
ATTN CODE 753, LIB DIV

COMMANDER
EDGEWOOD ARSENAL
EDGEWOOD ARSENAL, MD 21010
ATTN SMUEA-W, WEAPONS DEVELOPMENT &
ENGINEERING LABORATORIES

COMMANDER
ROCK ISLAND ARSENAL
ROCK ISLAND, IL 61201
ATTN SARRI-L, DR R BECKETT

DIRECTOR
USA BALLISTIC RESEARCH LABORATORIES
ABERDEEN PROVING GROUND, MD 21005
ATTN INTERIOR BALLISTICS LAB
ATTN EXTERIOR BALLISTICS LAB
ATTN TERMINAL BALLISTICS LAB
ATTN LIBRARY

COMMANDER
NAVAL ORDNANCE SYSTEMS COMMAND, HQ
2521 JEFFERSON DAVIS HIGHWAY
ARLINGTON, VA 20360
ATTN NORD-035, WEAPONS & DYNAMICS

COMMANDER
ARMAMENT DEVELOPMENT & TEST CENTER
EGLIN AIR FORCE BASE, FL 32542
ATTN DL, AF ARMAMENT LABORATORY
ATTN DLD, GUNS & ROCKETS DIVISION
ATTN ADTC (DLOSL), TECH LIBRARY

COMMANDER
HQ AIR FORCE SYSTEMS COMMAND
ANDREWS AFB
WASHINGTON, DC 20331

HARRY DIAMOND LABORATORIES
ATTN MCGREGOR, THOMAS, COL, COMMANDING
OFFICER/FLYER, I.N./LANDIS, P.E./
SOMMER, H./CONRAD, E.E.
ATTN CARTER, W.W., DR., ACTING
TECHNICAL DIRECTOR/MARCUS, S.M.
ATTN KIMMEL, S., PIO
ATTN CHIEF, 0021
ATTN CHIEF, 0022
ATTN CHIEF, LAB 100
ATTN CHIEF, LAB 200
ATTN CHIEF, LAB 300
ATTN CHIEF, LAB 400
ATTN CHIEF, LAB 500
ATTN CHIEF, LAB 600
ATTN CHIEF, DIV 700
ATTN CHIEF, DIV 800
ATTN CHIEF, LAB 900
ATTN CHIEF, LAB 1000
ATTN RECORD COPY, 041
ATTN HDL LIBRARY (3 COPIES)
ATTN CHAIRMAN, EDITORIAL COMMITTEE
ATTN CHIEF, 047
ATTN TECHNICAL REPORTS, 013
ATTN PATENT LAW BRANCH, 071
ATTN MCLAUGHLIN, P.W., 741
ATTN CHIEF, BR 410
ATTN CHIEF, BR 420
ATTN RICHMOND, L, 420
ATTN OVERMAN, D, 420
ATTN CHIEF, BR 430
ATTN CHIEF, BR 440
ATTN CHIEF, BR 850
ATTN DAVIS, H., BR 850 (5 COPIES)
ATTN CHIEF, BR 940